
Article:
Liu, B., He, S. orcid.org/0000-0003-0326-2447, Moulinec, C. et al. (1 more author) (2019) Sub-channel CFD for nuclear fuel bundles. Nuclear Engineering and Design, 355. 110318. ISSN 0029-5493

https://doi.org/10.1016/j.nucengdes.2019.110318

Sub-Channel CFD for Nuclear Fuel Bundles

B. Liu [a,*], S. He [a], C. Moulinec [b] and J. Uribe [c]

[a] Department of Mechanical Engineering, University of Sheffield, Sheffield, S1 4DE, UK

[b] Science and Technology Facilities Council, Daresbury Laboratory, Warrington, WA4 4AD, UK

[c] EDF Energy R&D UK Centre, Manchester, M13 9PL, UK

[*] Correspondence: bo.liu@sheffield.ac.uk

Abstract

This paper presents a novel Computational Fluid Dynamics (CFD)-based sub-channel framework for nuclear power plants, which combines the advantageous features of modern CFD and traditional 1-D sub-channel codes. The new method is capable of producing CFD-level 3-D results with locally desirable refinement when coupled with embedded resolved models, but because a very coarse mesh is used over most part of the domain, the computing cost is typically significantly smaller than that of a conventional CFD simulation.

In this new Sub-Channel CFD (SubChCFD), a dual-mesh system is used, comprising, (i) a filtering mesh which aligns with the mesh used in typical sub-channel codes, enabling the use of existing engineering correlations to account for integral wall friction and heat transfer effects, and (ii) a computing mesh, which provides a platform for the solution of the governing equations with turbulence modelled using a mixing-length-type model. The method has been implemented in an open-source finite volume CFD code Code_Saturne and validated initially using a 5×5 bare bundle case based on the OECD/NEA MATiS-H benchmarking experiment. It has been found that SubChCFD is able of satisfactorily predicting both the velocity and temperature fields. To further investigate the performance for complex flow conditions, SubChCFD was applied to two full 3-D cases. The first is a 5×5 rod bundle case with local blockage in one of the sub-channels, creating significant localised cross flows. The second is a two-parallel-assembly channel with different input mass flow rates at the inlet of each assembly, allowing strong inter-assembly mixing. For both cases, SubChCFD has produced results which agree well with experiments and simulations using resolved CFD. It has also been demonstrated that SubChCFD exhibits excellent flexibility in comparison with traditional sub-channel codes and that it has the potential to serve as a substitution to sub-channel codes.

Keywords

Nuclear reactor, CFD, Heat transfer, Sub-Channel, Coarse-Grid

1. Introduction

To leverage the aggravation of the global environmental crisis, such as global warming and climate change, arising from the consumption of carbon-based fuel, nuclear power will continue to play an important role in energy generation due to its low emission of greenhouse gases. There are currently about 440 nuclear power plants in operation around the world and over 120 new reactors under construction (Moorthi et al., 2018). Following lessons learned from some major nuclear accidents, especially the most important one in Fukushima in 2011, passive cooling and margin management have proven to be increasingly prominent. In addition to steady-state normal operating conditions, safety assessment of the modern nuclear system needs to consider a variety of additional scenarios, such as: operational transients (e.g. start-up, and shut-down); anticipated off-design operation (for activities such as refuelling) and a wide variety of postulated fault and accident conditions, to enable fault recovering strategies to be developed and also to minimise the risk of radiological release.

The safety assessment of a nuclear reactor core and its associated components strongly relies on thermal hydraulic analysis of the coolant by means of experimental investigation or numerical simulations (Sha, 1980; Yadigaroglu et al., 2003). Restricted by the computational power in the 1960s to 1980s, the thermal hydraulic calculations were mainly performed using the best-estimate system codes such as RELAP5 (RELAP5 Development Team, 1995), ATHLET (Lerchl et al., 2012), CATHARE (Bestion, 1990) and TRAC (Liles and Mahaffy, 1986), and sub-channel codes such as COBRA (Rowe, 1967), VIPRE (Stewart et al., 1983) and MATRA (Hwang et al., 2008).The former are usually used to analyse the overall behaviour of the whole system under different operating conditions, whereas the latter provide a relatively detailed thermal hydraulic analysis at the fuel channel level by solving 1-D transport equations based on individual flow passages formed between fuel rods or fuel rods and walls, i.e. the so-called sub-channels. These transport equations are based on empirical correlations to account for un-resolved physics, such as frictional loss, spacer induced effects, turbulence, inter-channel mixing, and void drifting, etc. As such, sub-channel analysis codes are able to provide numerical predictions at a resolution of the sub-channel scale, which was state-of-the-art in 1-D approaches at that time. However, it is more and more likely that traditional 1-D codes are no longer sufficient in meeting the requirements of modern reactor design and safety case development (Brockmeyer et al., 2016; Jeong et al., 2005), despite the fact that they are able to provide an answer quickly. The rapid increase in computational power in the last several decades allows the advanced Computational Fluid Dynamics (CFD) methods to be used by reactor developers to study some complex 3-D physics of coolant flow in nuclear fuel channels. This has the potential to significantly re-shape future nuclear thermal hydraulic analysis.

Due to the complex internal structure, the scales of the flow in a nuclear reactor span a large range, varying from sub-millimeter (e.g. secondary flow in fuel assemblies) to meters or even tens of meters (e.g. natural circulation in a loss of coolant accident (LOCA)) (Yu et al., 2017). This requires the computational domain of a CFD model to be meshed using a fine grid to allow most physical scales to be captured. Consequently, it is still not practical to carry out core-level CFD simulations due to the prohibitive computing expense even with today's high-performance computing systems. Alternatively, CFD simulations can be carried out for representative sections with properly defined boundary conditions to reduce the computing cost by taking advantage of the fact that the core structures are typically spatially periodic in a nuclear reactor. Such an approach has been used by various researchers to carry out CFD analysis for single channels (Cui and Kim, 2003; Házi, 2005; Imaizumi et al., 1995; Karouta et al., 1995), multiple channels (G. Chen et al., 2017; Han et al., 2017; Liu et al., 2012; Liu and Ferng, 2010; Tseng et al., 2014; Zhao et al., 2017), rod bundle arrays (Agbodemegbe et al., 2016; Ala et al., 2017; Bieder, 2017; Bieder et al., 2014; Denefle et al., 2017; Ikeda, 2014; Kang and Hassan, 2016), reactor core sectors (Simoneau et al., 2007; Takamatsu, 2017; Tsuji et al., 2014), and plena (M. Kao et al., 2010; Kao et al., 2011), etc. With the experiences accumulated in academia, CFD is further used in industry to optimise the design of some key components of reactors, such as spacer grids of a Pressurised water reactor (PWR) fuel assembly (Ikeda, 2014; Podila et al., 2013). Among these studies and applications, the wall-function Reynolds averaged Navier-Stokes (RANS) methods, especially the k- ε series models were often used in early research (Cui and Kim, 2003; Házi, 2005; Imaizumi et al., 1995) or the modelling of large components (M. Kao et al., 2010; Kao et al., 2011; Simoneau et al., 2007; Takamatsu, 2017; Tsuji et al., 2014) as they can provide reasonable predictions at relatively small costs since the near-wall region is not resolved. However, the methods are no longer satisfactory for cases with complex flow phenomena, such as adverse pressure gradient, vortex shedding, impingement, swirling, and buoyancy influenced flows, etc. In such cases, more sophisticated methods are usually required for better predictions, such as anisotropic Reynolds-Stress Models (RSM) and low Reynolds number RANS or unsteady RANS models (X. Chen et al., 2017; M.-T. Kao et al., 2010) in which the boundary layer can be resolved down to the viscous sub-layer using high-resolution near-wall meshes with the first cell y+ up to 1.0. In addition, the state-of-the-art high-fidelity methods, e.g. Large Eddy Simulation (LES) and Direct Numerical Simulation (DNS) have also been used by many researchers in nuclear thermal hydraulics (Benhanmadouche et al., 2009; Fischer et al., 2007; Shams et al., 2013). Due to the extremely high cost of the latter methods, they cannot be widely used in engineering, especially DNS which is still restricted to simple geometries and low Reynolds numbers. However, they are normally used to generate benchmarking dataset for the development of new RANS turbulence models or as numerical tools for the fundamental study of turbulence.

Work has been done to make use of the advancement of modern CFD in core-level or even system-level modelling by coupling it with low cost simpler methods. In such approaches, CFD usually takes the role of capturing the complex 3-D flow of the most interesting regions/sections in the reactor system, whilst the rest is described using simplified models. The information exchange between the different models is challenging, which can be explicit or implicit in time and spatially decomposed or overlapped, depending on the method used (Grunloh and Manera, 2016).

At system level, CFD can be coupled to system codes to enhance their performance in predicting the complex behaviour of the entire nuclear power plant (NPP) under non-design conditions. To date, tremendous efforts have been dedicated to enabling the coupling between CFD and system codes. Anderson et al. (2008) analysed a very high-temperature reactor (VHTR) using a coupled RELAP/CFD system where the 3-D flow in the outlet plenum was modelled using CFD. Papukchiev et al. (2011) coupled ATHLET and ANSYS CFX, and then validations were done based on a pressure thermal shock related experiment for pressurized water-cooled reactor (PWR). Bury (2013) studied a reactor containment system under a scenario of LOCA using an in-house system code HEPCAL-AD coupled with ANSYS FLUENT. The natural circulation within an annular channel between an inner steel vessel and the containment wall was simulated using CFD. Bavière et al. (2014) simulated a sodium-cooled nuclear system with a coupled simulation of CATHARE2 and Trio_U, which allows energy and momentum feedback from CFD to the system code. Toti et al. (2017) implemented an implicit domain decomposition algorithm to enable the coupling between the system code RELAP5-3D and ANSYS FLUENT for high fidelity safety analyses of pool-type reactors. The method showed good agreement with the experimental data of a loss of flow transient induced by local 3-D phenomena. Despite the encouraging progress, there are two challenges in such code couplings. One is the low convergence rate due to the weak coupling, e.g. using a time explicit scheme in which the information is only exchanged once at the end of each time step. The other major challenge is that it is difficult to develop a generic library that can be used for different pairs of coupling codes, because of their very different data structures.

At core-level, one of the most popular approaches used in the open literature is to couple the porous media model with the well-resolved CFD to reduce the computing cost. In some of the cases, porous media is used to describe fuel assemblies (Chen et al., 2015; Fiorina et al., 2015; Skibin et al., 2017; Yu et al., 2015), others also include plena (Brewster et al., 2017; R. Chen et al., 2017). Some researchers have developed alternative ways to simplify the core modelling. For example, Corzo et al. (2015) incorporated a 1-D finite volume code to account for the complex fuel channels in a full core simulation of a pressurised heavy water reactor. Zhang et al. (2013) employed a distributed resistance model to represent the core module of a real geometry model of a PWR, whilst a detailed model was used for the down-comer and

the lower plenum. These simplified methods are, to some extent, similar to sub-channel codes, in which either the flow is forced in a single direction, or the geometry of the fuel rods is not taken into account explicitly. As such, these approaches are not suitable to capture small to medium scaled 3-D transient features, for example, the recirculation behind a blockage.

A new interesting area of research is the development of unresolved, coarse grid CFD to enable relatively large flow systems to be simulated at a low cost. Along this line of research, Hu and Fanning (2013) introduced a 3-D momentum source term method to simulate anisotropic flows in fuel channels of wire-wrapped bundles without fully resolving the geometrical details of the wires with fine meshes. Bieder et al. (2010) also studied wire-wrapped bundles using a low-resolution method, but differing from Hu and Fanning. They simplified the mesh generation by replacing the wire wrap with a spinal fin. Roelofs et al. (2012) proposed a method referred to as Low-Resolution Geometry Resolving (LRGR) CFD which captures 'medium scale' flow features without a sub-grid model in the case that secondary flows are not important. Class et al. (2011) and Viellieber and Class (2012) employed an even coarser mesh in their approach, referred to as Coarse-Grid CFD (CG-CFD), to make the simulation as efficient as sub-channel codes but without depending on experimental data. They solve the Euler equations instead of the Navier-Stokes equations with diffusion effects accounted for using a volumetric force extracted from detailed simulations pre-performed on the same geometry. This approach has to date not been applied to heat transfer where the parametric procedure could be a challenge due to the coupling between momentum and energy transport. Along a totally new line, Hanna et al. (2017) associated the local error arising from grid coarsening to features of the mesh by training a surrogate statistical model with detailed simulation results using the state-of-the-art machine learning technology and then tested their method on a 3D lid-driven cavity flow.

In conclusion, although great advances have been made in CFD over the past few decades, which enable many problems previously only tackled by experiments to be solved by means of numerical simulation (thus saving considerable resources), the application of CFD in real-life engineering is still limited by its high computing cost. Additionally, CFD is a generic tool which is not developed specifically for nuclear applications. The uncertainties related to numerical strategies, user inputs (e.g., initial and boundary conditions), and turbulence models are very difficult to measure and control due to the generality, complexity and flexibility of the method. For these reasons, reactor design and safety assessment in the nuclear industry still largely rely on system and sub-channel codes.

To make use of the modelling techniques achieved in the booming development of CFD in nuclear thermal-hydraulic modelling to supplement or potentially replace the lower-order methods, an effective solution may be to implement some key concepts of the 1-D methods in the framework of modern CFD.

In doing so, the traditional 1-D tools could be modernised to have some CFD-like features with improved flexibility, while maintaining the strengths of the system/sub-channel codes so as to provide performance and accuracy that are at least as good as the system/sub-channel codes without a significant increase in computing cost. Thanks to the use of the CFD platform, this approach will have the potential to be easily coupled with traditional CFD methods, thus circumventing a series of difficulties and problems encountered in coupling between different platforms.

The purpose of this paper is to present a novel coarse grid CFD technique following the aforementioned approach. Unlike the methodology of other coarse grid CFD, e.g., Class et al. (2011), Viellieber and Class, (2012) and Hanna et al. (2017), which is aimed at alleviating the dependence on experiments and empiricism, our method can best be described as a low-resolution CFD using a correlation-based model closure method, in which the experimental and engineering data are used whenever possible. In this method, the inviscid flow with corrections for mixing is solved on a very coarse grid using a standard CFD solver while the empirical correlations of the frictional loss and heat transfer are used to ensure correct integral effects of the solid walls.

Section 2 introduces the methodology of the novel coarse grid CFD, Section 3 presents its validation and application to several test cases and Section 4 provides some recommendations.

2. Methodology

The novel method presented herein is a new coarse grid CFD solver coupled with an embedded sub-channel model, which is referred to as sub-channel CFD or SubChCFD. The method adopts a dual mesh/dual solution methodology, namely, (i) a filtering mesh which aligns with the mesh used in typical sub-channel codes, enabling the integral wall friction and heat transfer effects calculated using existing engineering correlations, and (ii) a computing mesh, on which the RANS equations with a simple mixing length-type model are solved. The former is also referred to as the sub-channel mesh/calculation and the latter to the CFD mesh/solution. The friction and heat transfer calculated from the sub-channel solution are used in the CFD via boundary conditions to ensure that the integral effect of the flow solution is consistent with existing engineering correlations. On the other hand, the detailed CFD results are integrated over the sub-channel cells to produce the integral flow parameters (e.g. velocity, thermal properties), which are used in the sub-channel calculations.

The mapping between the filtering mesh and the computing mesh is established through geometrical relations so that any physical parameters and field variables stored on the latter can be used directly to produce corresponding sub-channel quantities for the former by spatial averaging, i.e.

194 $$\varphi_{sub,j} = \sum_{i \in j} \left(\frac{V_i}{V_{sub,j}} \right) \varphi_i \quad (1)$$

195 where $\varphi_{sub,j}$ is the sub-channel-level quantity of φ on the j^{th} filtering mesh element, φ_i the CFD-level
196 quantity of φ on the i^{th} computing mesh element, V_i the volume of the i^{th} computing mesh element, $V_{sub,j}$
197 the volume of the j^{th} filtering mesh element.

198 With the advancement of the iteration process, information is continually exchanged between the
199 computing mesh and the filtering mesh, and finally, the CFD solution obtained and the empirical
200 correlations at the sub-channel level are consistent with each other. In practice, this can be achieved when
201 the CFD solver reaches convergence on the computing mesh, because the correlations are used as
202 boundary conditions in the CFD simulation. The detailed procedure of the algorithm of SubChCFD is
203 presented in Figure 1.

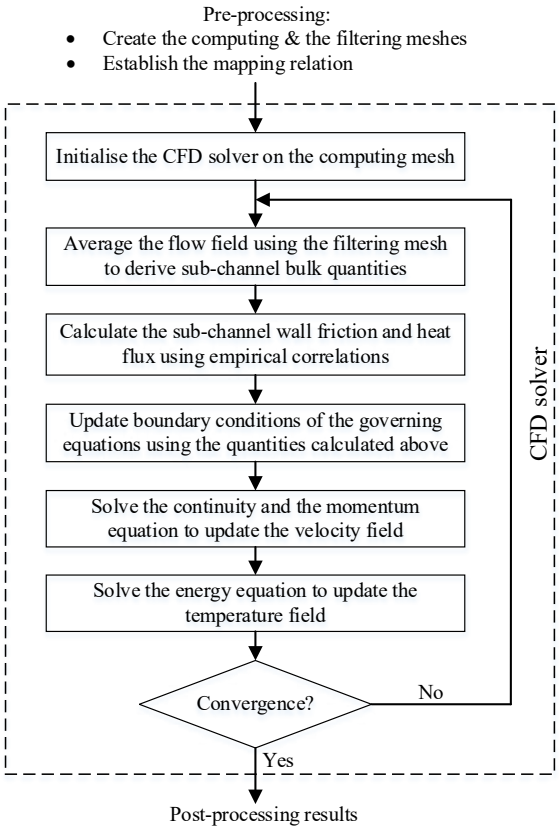

204

205 **Fig. 1 Details of the SubChCFD methodology**

206 The RANS governing equation to be solved in SubChCFD can be expressed as

$$\frac{\partial \rho \vec{u}}{\partial t} + \nabla \cdot \rho \vec{u} \otimes \vec{u} = -\nabla p + \nabla \cdot \bar{\sigma} + \vec{S}_u \tag{2}$$

where $\bar{\sigma}$ is the stress tensor including both the viscous and the turbulence contributions, $\vec{S}_u$ is the body force. The discrete form is derived by integrating Equation (2) over each computing mesh cell Ω to yield:

$$\begin{aligned} \iiint_{\Omega} \frac{\partial \rho \vec{u}}{\partial t} dV + \oiint_{S} \vec{u} \left(\rho \vec{u} \cdot \vec{n} \right) dA &= -\oiint_{S} \left(\bar{I} p \cdot \vec{n} \right) dA + \oiint_{S} \bar{\sigma} \cdot \vec{n} dA + \iiint_{\Omega} \vec{S}_u dV \\ &= -\oiint_{S} \left(\bar{I} p \cdot \vec{n} \right) dA + \iint_{S_w} \bar{\sigma} \cdot \vec{n} dA + \iint_{S_f} \bar{\sigma} \cdot \vec{n} dA + \iiint_{\Omega} \vec{S}_u dV \end{aligned} \tag{3}$$

where $S = S_w \bigcup S_f$, S_w is the cell surfaces adjacent to a wall boundary, S_f is the interior cell surfaces. The convection term is discretised directly, whereas the viscous term requires some special care. During the Stokes integration, the viscous term is decomposed into two parts which include the wall boundaries and the interior interfaces, describing viscous forces between the wall and the adjacent fluid element and viscous forces between fluid elements, respectively. Figure 2 shows an example of the mesh system used for a PWR fuel channel where the physical meaning of the two parts of the viscous term is also clearly demonstrated.

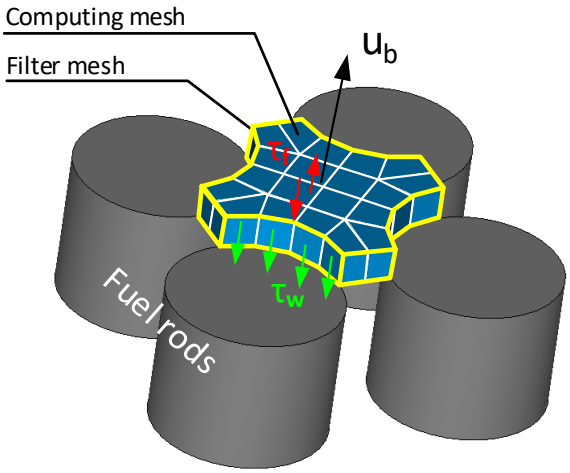

Fig. 2 Mesh system in SubChCFD

Since the mesh used in SubChCFD is very coarse, all the control volumes in the computational domain can be safely assumed to be located in the core flow region sufficiently away from the wall effect. Therefore, the discretisation of the interior part of the diffusion term, i.e. the second last term in Equation (3), is not expected to have significant errors thanks to the relatively low velocity gradients occurring

there. The eddy viscosity is modelled using a simple model such as a 0-equation mixing length turbulence model, which is used in this study. As such, the interior part can be finally written in the following form and discretised.

$$\iint_{S_f} \bar{\sigma} \cdot \vec{n} dA = \iint_{S_f} \left(\mu + \mu_t\right)\left(\nabla \vec{u} + \nabla \vec{u}^T - \frac{2}{3}\delta \nabla \cdot \vec{u} \right) \cdot \vec{n} dA \tag{4}$$

where $\mu_t = \rho {l_m}^2 \sqrt{2 S_{ij} S_{ij}}$, the mixing length l_m can be calculated through l_m=0.09Δ (Δ is the thickness of the boundary layer, which takes a value of half the hydraulic diameter in bundle flows).

The wall-boundary part of the diffusion term, i.e. the third last term of Equation (3), can be calculated as follows,

$$\iint_{S_W} \bar{\sigma} \cdot \vec{n} dA = \frac{1}{4} f \frac{1}{2} \rho_b \vec{u}_b \left|\vec{u}_b\right| \iint_{S_W} dA \tag{5}$$

where f denotes the skin fractional factor; ρ_b and $\vec{u}_b$ represent the sub-channel bulk density and bulk velocity, respectively.

The energy equation,

$$C_p \left(\frac{\partial \rho T}{\partial t} + \nabla \cdot \rho \vec{u} T \right) = -\nabla \cdot \vec{q} + S_E \tag{6}$$

is treated in a similar way to generate an integrated form. It reads

$$\begin{aligned} C_p \left(\iiint_{\Omega} \frac{\partial \rho T}{\partial t} dV + \oiint_{S} \vec{u}\left(\rho T \cdot \vec{n}\right) dA \right) &= -\oiint_{S} \vec{q} \cdot \vec{n} dA + \iiint_{\Omega} S_E dV \\ &= -\iint_{S_w} \vec{q} \cdot \vec{n} dA - \iint_{S_f} \vec{q} \cdot \vec{n} dA + \iiint_{\Omega} S_E dV \end{aligned} . \tag{7}$$

The diffusion term of the energy equation is also split into a wall-boundary part and an interior part. The interior part is calculated using

$$\iint_{S_f} \vec{q} \cdot \vec{n} dA = -\iint_{S_f} \left(\lambda + \lambda_t\right) \nabla T \cdot \vec{n} dA . \tag{8}$$

The diffusion term in the energy equation at the wall boundaries is determined using the sub-channel-based Nusselt number correlations. The calculation of the wall-boundary part depends on the types of the boundary condition of the solid walls. Table 1 shows the details of the calculation method for three different types of thermal boundary conditions. It can be noted that, for the Dirichlet and Robin boundary conditions, the Nusselt number is present in the calculation of the wall heat flux in the main solution loop for the governing equations. As depending on the flow at the sub-channel level, the Nusselt number can only be calculated using the information from the previous time step, that is, an explicit coupling between the sub-channel and CFD solutions. Here, the sub-channel bulk temperature T_b is calculated using the following equation,

$$T_b = \iiint_{\Omega_{sub}} \rho u T^{n-1} dV \Big/ \iiint_{\Omega_{sub}} \rho u dV \tag{9}$$

where T^{n-1} is the temperature at the previous time step, Ω_{sub} represents a cell of the filtering mesh.

The situation is much simpler for the case of the Neumann boundary condition as the wall heat flux is given. The Nusselt number is only required for estimating the surface temperature of the walls during the post-processing stage.

Table 1 Near-wall part of the diffusion term in the energy equation

Boundary types	Conditions	$\iint_{S_W} \vec{q} \cdot \vec{n} dA$
Dirichlet	$T\Big\|_{S_w} = T_w$	$-\frac{\lambda \mathrm{Nu}}{D_h}\left(T_w - T_b\right) \iint_{S_W} dA$
Neumann	$\left.\frac{\partial T}{\partial n}\right\|_{S_w} = -q$	$q \iint_{S_W} dA$
Robin	$\left.\left(aT + b\frac{\partial T}{\partial n}\right)\right\|_{S_w} = c$	$\frac{\lambda \mathrm{Nu}(aT_b - c)}{aD_h + b\mathrm{Nu}} \iint_{S_W} dA$

Due to the use of the coarse grid, SubChCFD is not expected to achieve complete mesh-independence of the solution even though as it will be shown later in this Section 3.1.2, SubChCFD has demonstrated rather small mesh-dependence. To further limit mesh-dependence, improve consistency in model

generation for different flow problems and improve the accuracy of the simulation, we note the following guidelines on mesh generation:

1. The filtering mesh should be chosen closely following the sub-channel divisions used in traditional sub-channel codes where possible.
2. The computing mesh should be generated from the filtering mesh, effectively sub-dividing it into smaller cells.
3. Each sub-channel is divided into two regions, namely, the wall region and the core region.
4. Taking square-lattice PWR sub-channel as an example, we suggest three 'standard' mesh strategies for a 2-D cross section mesh of the sub-channels as outlined below (see Figure 3). They can be used directly to build the full 3-D mesh by axial extrusion.
    a) Mesh 1: The wall region is represented by a single wall-layer, comprising 4×1 cells; and the core is meshed by a 2×2 mesh.
    b) Mesh 2: The wall region is represented by two wall layers, comprising 6×2 cells; and the core is meshed by a 2×2 mesh.
    c) Mesh 3: The wall region is represented by two wall layers, comprising 8×2 cells; the core is meshed by a 4×4 mesh.

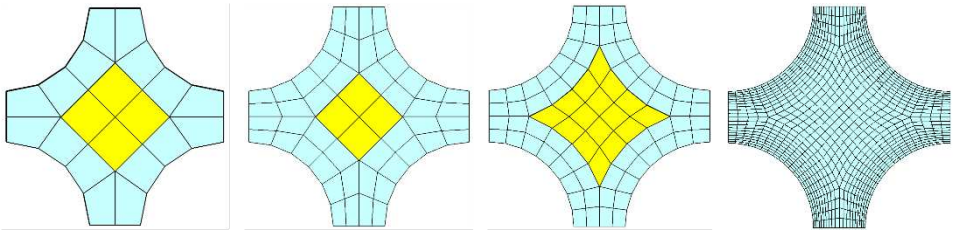

(a) Mesh-1 (b) Mesh-2 (c) Mesh-3 (d) CFD mesh

Fig. 3 Comparison of the computing mesh set in SubChCFD and a RANS wall-modelled CFD mesh for a square-lattice PWR sub-channel

The aforementioned mesh strategies allows SubChCFD to have a higher flexibility than the traditional 1-D tools in capturing flow physics. It is expected that the users of SubChCFD will select a suitable strategy for their purpose to balance resolution requirements and computing cost and will maintain the same mesh for their application. In practice, the model parameters used in SubChCFD will be pre-calibrated taking into account the mesh strategies to ensure an optimal performance when used for a specific type of nuclear reactor. Figure 3 gives an example of the computing mesh set generated in line with the above mesh strategies (see Mesh-1, Mesh-2, Mesh-3 on Figure 3 a, b and c, respectively) and a wall-modelled CFD mesh for a square-lattice PWR sub-channel (see Figure 3 d). It can be seen clearly that the cell count in

SubChCFD is much smaller than that in the conventional CFD (in this case, 20, 52 and 80 cells in Mesh 1, 2 and 3, while 624 cells in the CFD mesh). Accordingly, the computing cost is expected to be reduced by about 1 to 2 orders of magnitude in a 2-D case and 2 to 3 orders of magnitude in a full 3-D case, respectively. This is just a comparison with the wall-modelled CFD, and the reduction in computing cost will be even more significant when compared with wall-resolved CFD simulations.

3. Validation and Application

In this study, the multi-purpose CFD package Code_Saturne developed by EDF R&D (Fournier et al., 2011) is used as the platform to implement SubChCFD. Code_Saturne is a finite-volume method based open-source software, providing the user full access to the source code. A well-defined user subroutine system allows the user to implement self-defined models and methods easily and conveniently.

3.1 Fully developed flow and heat transfer in a 5×5 PWR bundle

3.1.1 Description of the test case

To demonstrate and validate the new methodology of SubChCFD in nuclear thermal-hydraulic modelling, a 2-D model is firstly created to simulate an axially fully developed flow in a rod bundle. The geometry of the bundle is taken from the OECD/NEA MATiS-H benchmarking experiment (Smith et al., 2013) in which the test section consists of a 5×5 rod bundle enclosed in a square housing. The geometrical features of the experimental rig are very similar to a real PWR fuel assembly, although the overall size is about three times bigger than the latter. Figure 4 shows some details of the cross section of the rod bundle. The working fluid used in the experiment is water at a bulk temperature T_0 of 35 °C, an operating pressure of 1.5 bar, and a bulk velocity u_0 of 1.5 m/s, corresponding to a Reynolds number of 50,250. In the original experiment, no heating was applied to the rods. In the simulation, however, we impose a 200 kW/m^2 heating to the surface of the rods to evaluate the behaviour of SubChCFD for heat transfer predictions. For the sake of simplicity, we assume that the density change due to temperature rise is negligible so that the momentum transport is not strongly coupled with heat transfer. In order to assist the validation process, a resolved CFD model has also been created for the same geometry to provide reference results in addition to the experimental data including data for heat transfer. The computing mesh and the filtering mesh of the rod bundle used in SubChCFD are shown in Figures 5 (a) and (b), respectively. It should be noted that the computing mesh is generated based on Mesh-1 described in Figure 3. Figure 5 (c) is the mesh used in the reference resolved CFD model. Since the flow inside the rod bundle is a wall-bounded shear flow, the standard k-ε turbulence model and the scalable wall function are sufficient to produce reliable reference results.

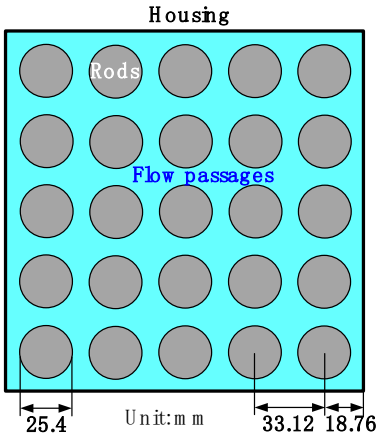

Fig. 4 Sketch of the 5x5 rod bundle

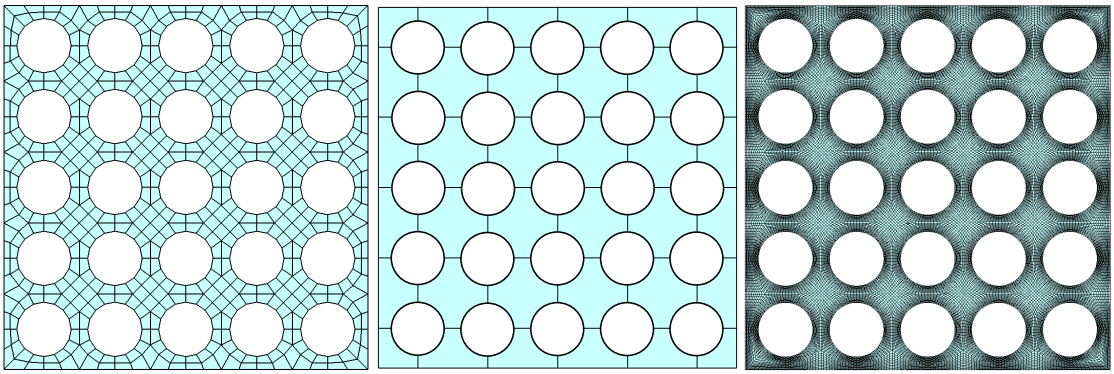

(a) (b) (c)

Fig. 5 Meshes used in the simulation, including (a) the computing mesh of SubChCFD, (b) the filtering mesh of SubChCFD, and (c) the CFD mesh of the reference model

Considering the fact that the flow studied here is fully developed in the axial direction (also called stream-wise direction), periodic conditions are imposed to the boundaries perpendicular to the rods and only one layer of cells is used in the stream-wise direction, which makes the model effectively 2-D. For momentum, full-slip wall boundaries are enabled by applying zero-gradient conditions to all the solid walls, whereas an empirical correlation of the frictional factor

$$f = \left[a + b_1 \left(\frac{P}{D_h} - 1 \right) + b_2 \left(\frac{P}{D_h} - 1 \right)^2 \right] / \mathrm{Re}^n \tag{10}$$

is used to calculate the wall friction which is further imposed as a momentum source term to the wall adjacent cells to account for the wall shear effect.

Table 2 gives the values of the parameters in the friction factor correlation for different types of sub-channels in a square-lattice rod bundle (Todreas and Kazimi, 1990).

Table 2 Parameters in the frictional factor correlation for square-lattice rod bundles

Sub-channel type	a	b_1	b_2	n
Interior (laminar)	35.55	263.7	-190.2	1
Edge (laminar)	44.40	256.7	-267.6	1
Corner (laminar)	58.83	160.7	-203.5	1
Interior (turbulent)	0.1339	0.09059	-0.09926	0.18
Edge (turbulent)	0.143	0.04199	-0.04428	0.18
Corner (turbulent)	0.1452	0.02681	-0.03411	0.18

An energy sink term is introduced to the energy equation to continuously remove a certain amount of heat which is in balance with that generated by the fuel rods so that a steady-state temperature field can be finally obtained. The energy sink is based on the computing mesh and can be calculated as follows,

$$S_E = \frac{\Phi_{net}\vec{u}\cdot\vec{e}_z}{\int_{\Omega_d}\vec{u}\cdot\vec{e}_z dV} \quad \frac{\Phi_{net}u_z}{\int_{\Omega_d}\vec{u}_z dV} \tag{11}$$

where Φ_{net} is the net heat input to the fluid, $\vec{e}_z$ is the unit vector of the stream-wise direction, Ω_d represents the whole computational domain.

Since the Neumann type thermal boundary condition is used for all the solid walls in this case, as discussed in Section 2, the Nusselt number does not enter the main simulation loop and is only used at the post-processing stage to estimate the surface temperature of the fuel rods. The wall temperature is calculated based on the filtering mesh using the following equation,

$$T_w = T_b - \frac{qD_h}{\lambda \mathrm{Nu}} \tag{12}$$

The Nusselt number correlation used here for the rod bundle is derived as a product of $(\mathrm{Nu}_\infty)_{c.t.}$ for the circular pipe in fully developed conditions multiplied with a correction factor (Todreas and Kazimi, 1990).

$$\mathrm{Nu} = \psi(\mathrm{Nu}_\infty)_{c.t.} \tag{13}$$

where $\psi = 1 \quad 0.9120\,\mathrm{Re}^{-0.1}\,\mathrm{Pr}^{0.4}(1 \quad 2.0043e^{-B})$, $B=D_h/D$.

$(\mathrm{Nu}_\infty)_{c.t.}$ is given by the Dittus-Boelter equation (Dittus and Boelter, 1985),

$$(\mathrm{Nu}_\infty)_{c.t.} = \begin{cases} 0.023\,\mathrm{Re}^{0.8}\,\mathrm{Pr}^{0.4} & \text{when the fluid is heated} \\ 0.023\,\mathrm{Re}^{0.8}\,\mathrm{Pr}^{0.3} & \text{when the fluid is cooled} \end{cases} \tag{14}$$

3.1.2 Standard geometry with uniform heating (base-line validation case)

Figure 6 shows the simulation results of SubChCFD and resolved CFD for the 5×5 rod bundle. It can be seen that SubChCFD is capable of capturing the main features of the velocity and temperature fields in the sub-channels really well. It is also clear that SubChCFD does not show the stagnation and the hot spots close to the wall predicted by the resolved CFD. This is expected because of the nature of this approach. Figure 7 provides a more detailed comparison using line plots, in which experimental data are also provided where available. It is first noted that the resolved CFD seems to overpredict the velocity variation between the rods measured in the experiment. The results of the SubChCFD model follow very closely these of the resolved CFD and also over-predict the temperature variations. Consequently, both models can successfully capture the overall trend of the flow pattern but both of them have similar deviations from the experimental measurements.

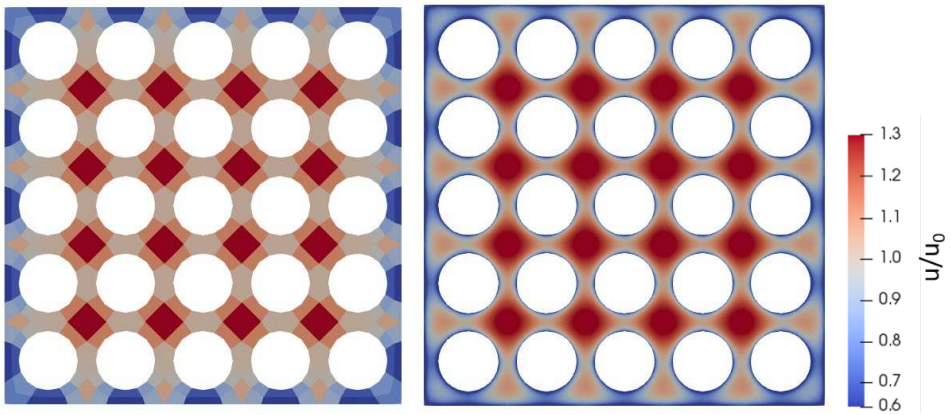

(a) (b)

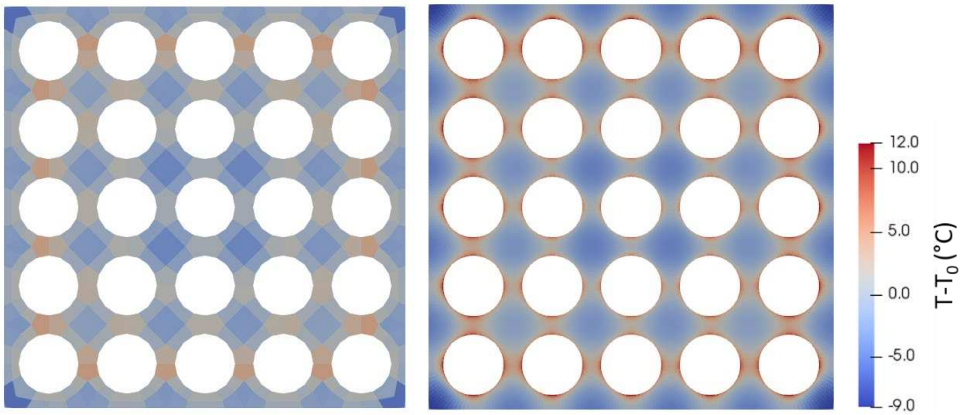

(c) (d)

Fig. 6 Contour plots of the 5×5 bundle, (a) and (b) the normalised axial velocity distribution derived from SubChCFD and resolved CFD simulations, (c) and (d) the temperature distribution derived from SubChCFD and resolved CFD simulations

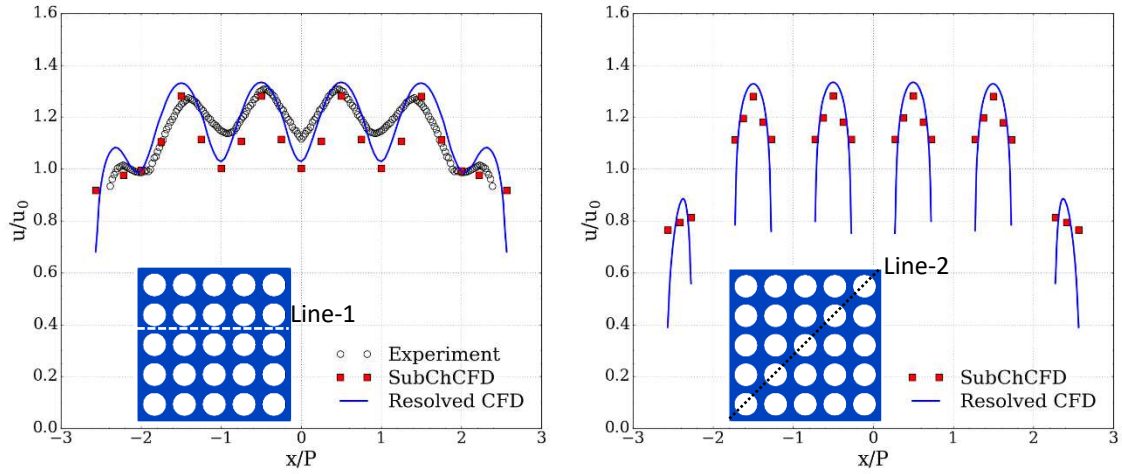

(a) (b)

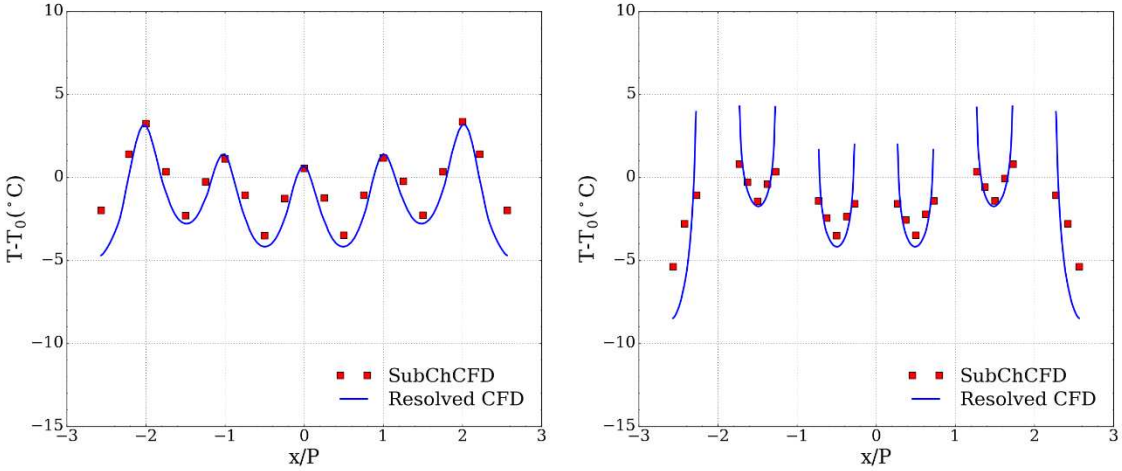

(c) (d)

Fig. 7 Line plots of the 5x5 bundle, (a) and (b) the normalised axial velocity over line-1 and line-2, (c) and (d) temperature over line-1 and line-2

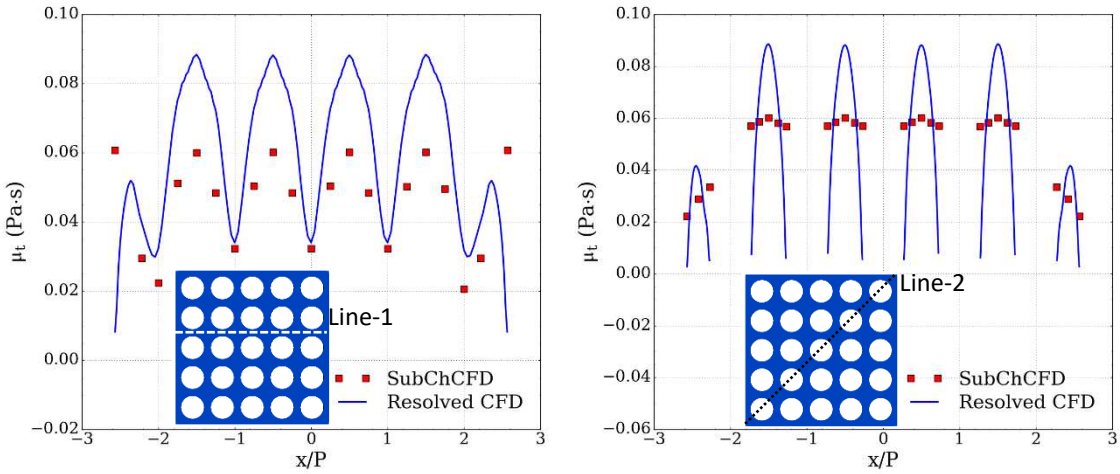

(a) (b)

Fig. 8 Line plots of the turbulent viscosity over (a) line-1 and (b) line-2

The good agreement between SubChCFD and the resolved model in capturing much of the details of the flow away from the wall implies that the mixing length model is capable of predicting a correct level of turbulence in the core region of the sub-channels using a very coarse grid. Figure 8 shows a comparison between the turbulent viscosities predicted by the two methods along the same lines where the velocity and temperature are plotted. Overall, SubChCFD gives very good results compared to the resolved model especially on line-2, where it reproduces the average value of the latter rather well. On line-1, SubChCFD seems to under-predict the turbulent level compared to the resolved model, but it is insignificant and has little effects on the overall flow field.

Figure 9 shows the circumferential distribution of the rod surface temperature. Fuel rods at four representative locations (including a corner rod, an edge rod and two interior rods) are selected for plotting the results. It is clear that each rod in the array belongs to four adjacent sub-channels simultaneously. Therefore, the calculation of the surface temperature of a fuel rod for a complete 360º is segmented, depending on four different sub-channel bulk temperatures. This is the reason why the SubChCFD result has a stepwise variation along the azimuthal direction. For better comparison, trend lines are added for the resolved CFD results by applying a box filter to spatially average the original data. It can be noted that SubChCFD cannot capture every detail of the surface temperature on the fuel rods as that in a typical resolved CFD simulation. However, the basic trends of the surface temperature distribution can be qualitatively predicted, even though there is a shift between the predictions of the two methods. Considering that the bulk temperature predictions are similar in the two methods, this shift implies that the Nusselt number correlation used in the SubChCFD does not agree well with the heat transfer predicted by the resolved model. The difference is moderate, between 10 to 20% of the wall-to-bulk temperature

difference. It should be noted that the correlation used in this case study is one of a generic form (Equations 13 & 14). In practice, the correlations used in SubChCFD are expected to be specifically developed for the particular fuel designs concerned. Ideally, such correlations will be derived from experiments, but more recently, CFD simulations have been used to extend the range of conditions of the database produced from experiments with reasonable success.

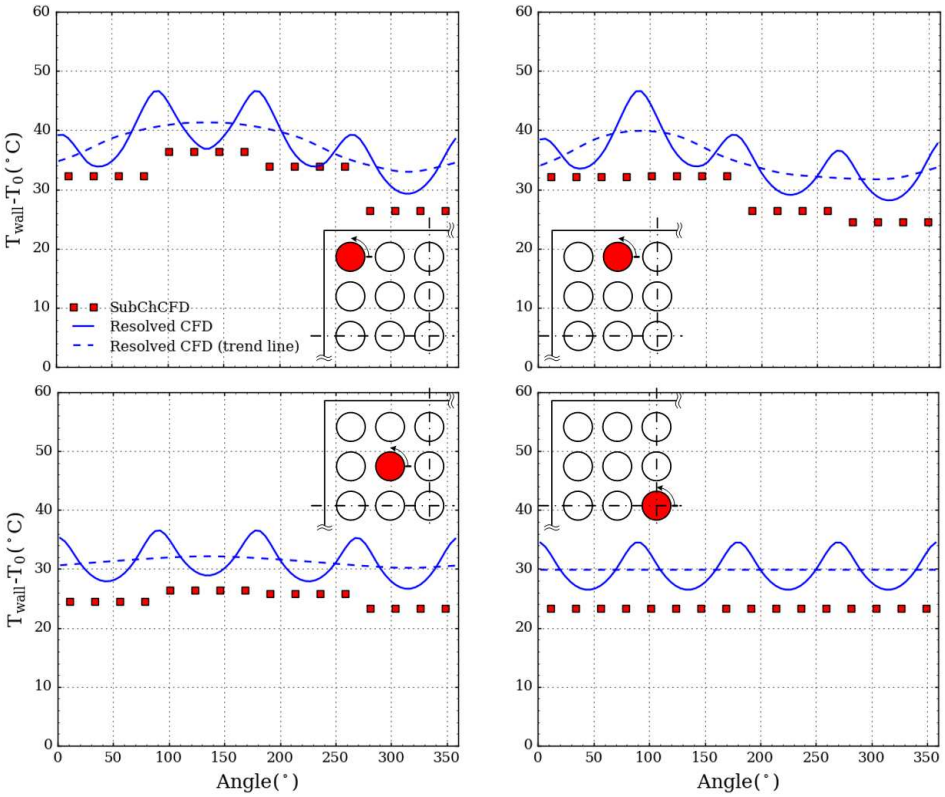

Fig. 9 Circumferential distribution of the surface temperature of the rods at representative locations. (The rod where the results are taken for plotting being highlighted in red)

A basic concern of the methodology developed for SubChCFD is the use of a standard CFD solver on a very coarse mesh, which may potentially cause significant discretisation error and consequent numerical diffusion. In order to evaluate the mesh-dependency of SubChCFD, two other computing meshes, based on resolutions of Mesh-2 and Mesh-3 (see Figure 3) respectively, are used to simulate the flow and heat transfer in the base-line case. The results are shown in Figure 10 and compared with the Mesh-1 result. It is interesting to observe that the results are nearly mesh independent although the Mesh-1 result slightly deviates from the other two meshes in some regions of the edge sub-channel and the corner sub-channel. Overall, the three meshes produce very similar results in terms of both velocity and temperature fields, which is especially the case for Mesh-2 and Mesh-3 results. This suggests that the numerical diffusion

related to the coarse mesh plays a relatively small role for this type of wall-bounded shear flows. However, it could be very significant in other cases and needs to be quantified wherever necessary in the future.

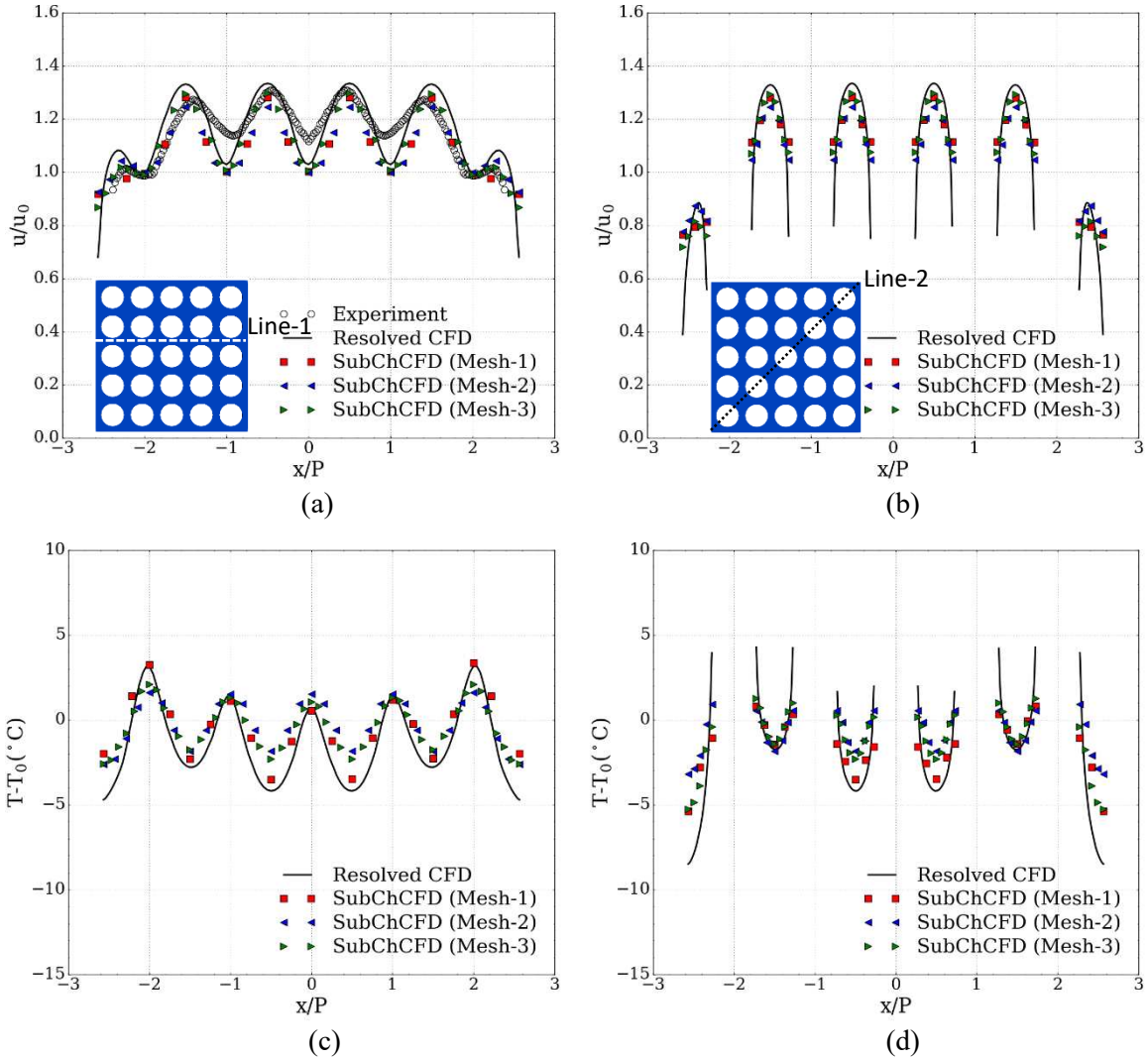

Fig. 10 Mesh-dependency test, (a) and (b) the normalised axial velocity over line-1 and line-2, (c) and (d) temperature over line-1 and line-2

To roughly compare the computing costs of SubChCFD and resolved CFD, serial simulations (using only 1 CPU processor) were run using the two methods, respectively, for a certain length of physical time at a fixed CFL number. Results obtained can be found in Table 3. As can be seen, the mean elapsed time per time step of SubChCFD is about only 1/60 that of resolved CFD due to the significant reduction in mesh size. Additionally, larger time step size is allowed at the same CFL number in SubChCFD because the local size of the mesh cells is larger, which results in an extra reduction in computing cost compared to

435 resolve CFD. Overall, the computing cost is saved by up to 560 times by using SubChCFD in this
436 particular case.

437 **Table 3 Evaluation of computing costs of Resolved CFD and SubChCFD**

Method	Mesh size (number of cells included)	Mean elapsed time per time step (s)	Mean time step size (s)	Elapsed time per physical time (s/s)
Resolved CFD	54,528	0.6369	0.001	636.9
SubChCFD	1,120	0.01184	0.0104	1.138

438

439 **3.1.3 Standard geometry with non-uniform heating**

440 To further assess the performance of SubChCFD, simulations have been carried out for two additional
441 flow scenarios derived by altering the distribution of the heating source and the geometrical layout of the
442 rods of the base-line validation case.

443 The first case is aimed at testing the performance of SubChCFD when applied to non-uniformly heated
444 bundles. This occurs in reactors, for example, following refuelling when fresh fuel sits next to the
445 boundary of partially spent fuel assemblies. For the sake of simplicity, a non-uniform thermal
446 environment is created in this test case by imposing a 200 kW/m^2 heat loading to the centre rod with all
447 other rods being teated as adiabatic. The flow condition in this case is exactly the same as that used in the
448 base-line validation case, so the velocity fields of the two cases are expected to be identical because there
449 is no feedback from the changed heat transfer circumstances to the momentum transport due to the use of
450 constant fluid physical properties. Hence, only the temperature results are presented in this section.
451 Figures 11 and 12 show the resulting temperature field predictions in forms of contour and line plots,
452 respectively. It can be seen that the temperature distribution predicted by SubChCFD agrees well with
453 that exhibited in the results of the resolved CFD in this non-uniform heating scenario. The large
454 temperature variations within the sub-channels adjacent to the heated rod are well captured by SubChCFD.
455 This is unlikely to be achieved using a traditional sub-channel code. In addition, the resolution of the
456 results can be controlled, to some extent, by employing different computing meshes. In this sense,
457 SubChCFD performs as flexible as a typical CFD approach.

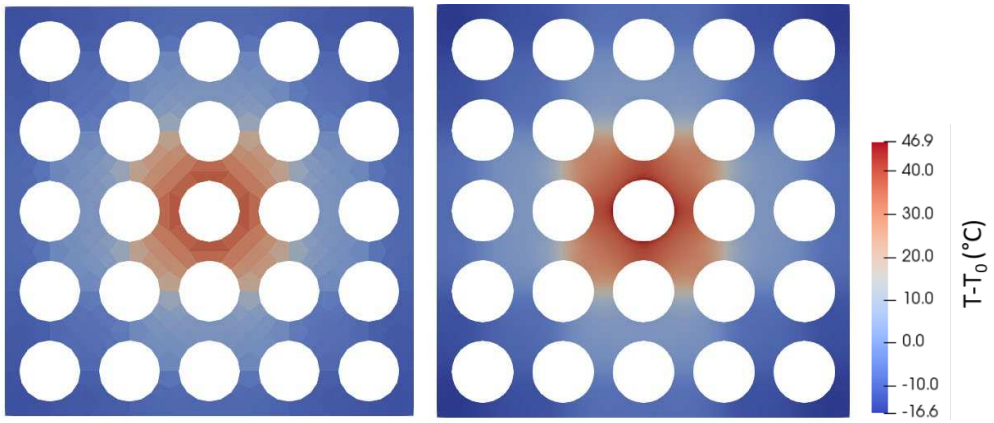

(a) (b)

Fig. 11 Temperature distribution of non-uniformly heated bundle obtained with (a) SubChCFD and (b) resolved CFD

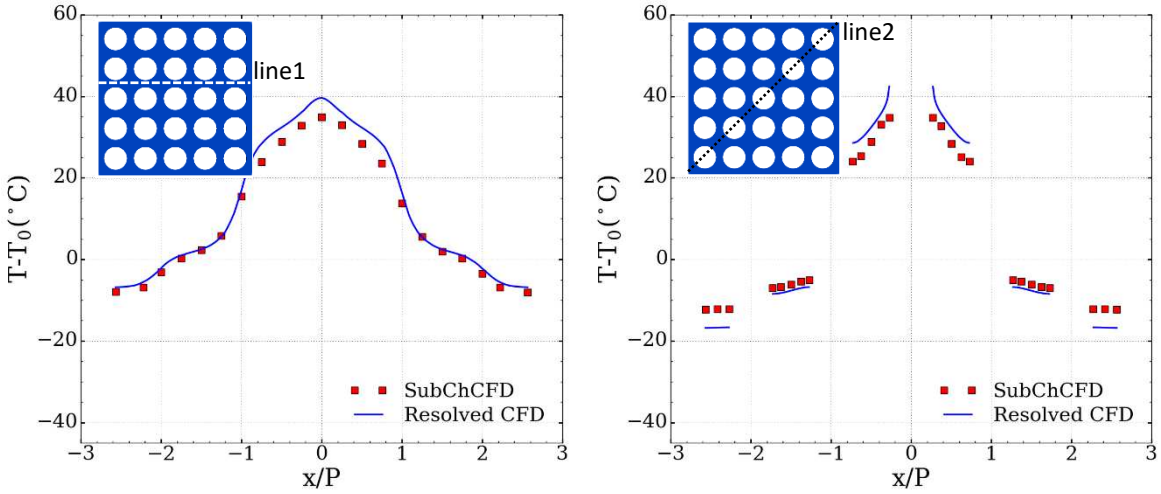

(a) (b)

Fig. 12 Line plots of the temperature field over (a) line 1 and (b) line2

3.1.4 Distorted geometry with uniform heating

The second case is aimed at testing SubChCFD for geometrically distorted rod bundles, which is also of great importance in engineering practice, especially for safety assessment. Here, we shift one column of the rods slightly to one side, creating a widened and a narrowed sub-channel on the two sides, respectively. The geometry change is expected to redistribute the mass flow among the sub-channels, leading to significant non-uniformity of the temperature distribution. Figures 13 and 14 show the simulation results of SubChCFD and the resolved CFD for the distorted rod bundle. It can be seen that SubChCFD responds to the geometrical change very well in terms of flow redistribution. The temperature redistribution has also been qualitatively captured, for example, the local increase in temperature caused by the reduction

of the coolant flow in narrow sub-channels, although the agreement could be further improved if required by calibrating some of the model parameters, such as the turbulent Prandtl number.

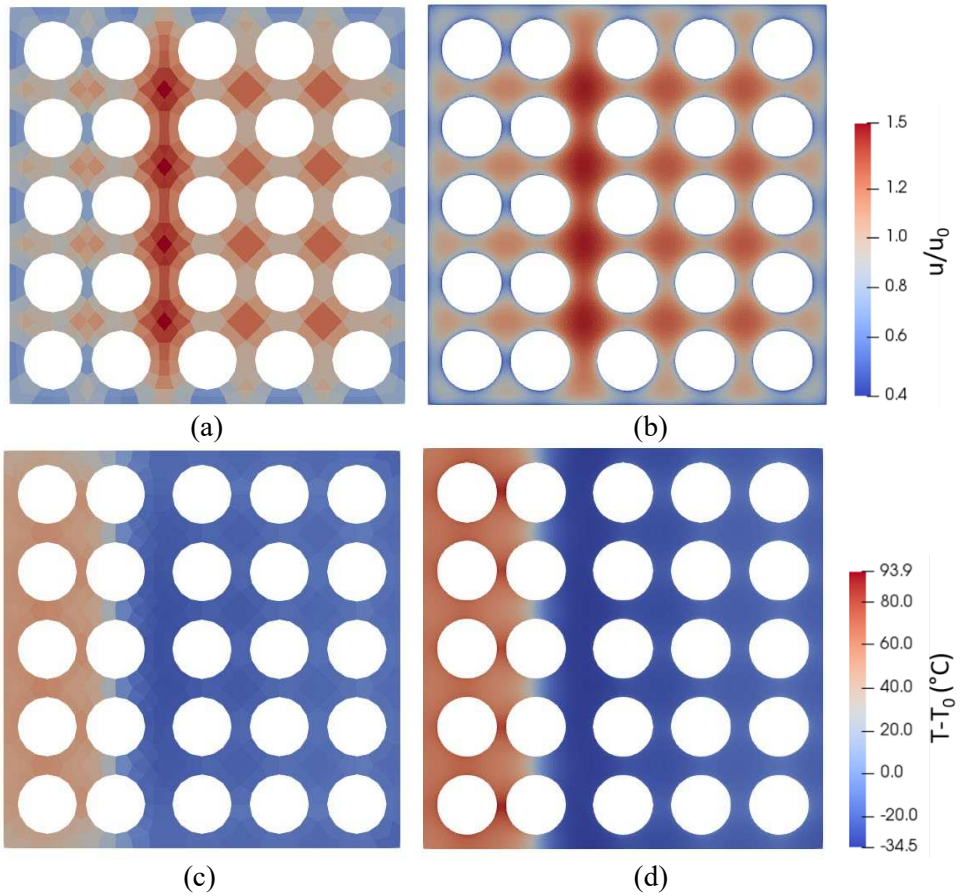

Fig. 13 Simulation results of the geometrically altered rod bundle, (a) and (b) the normalised axial velocity fields, (c) and (d) the temperature fields

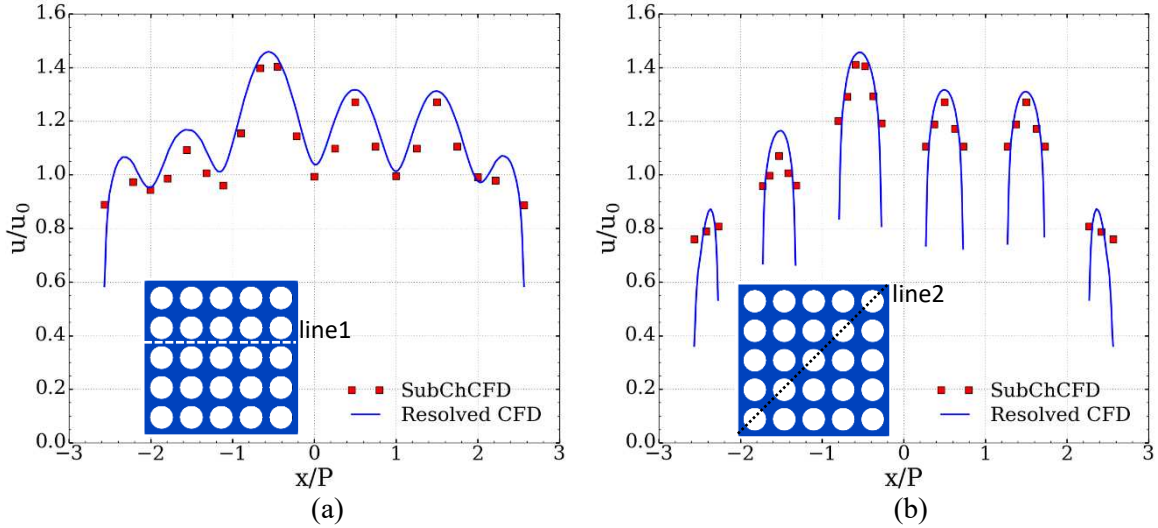

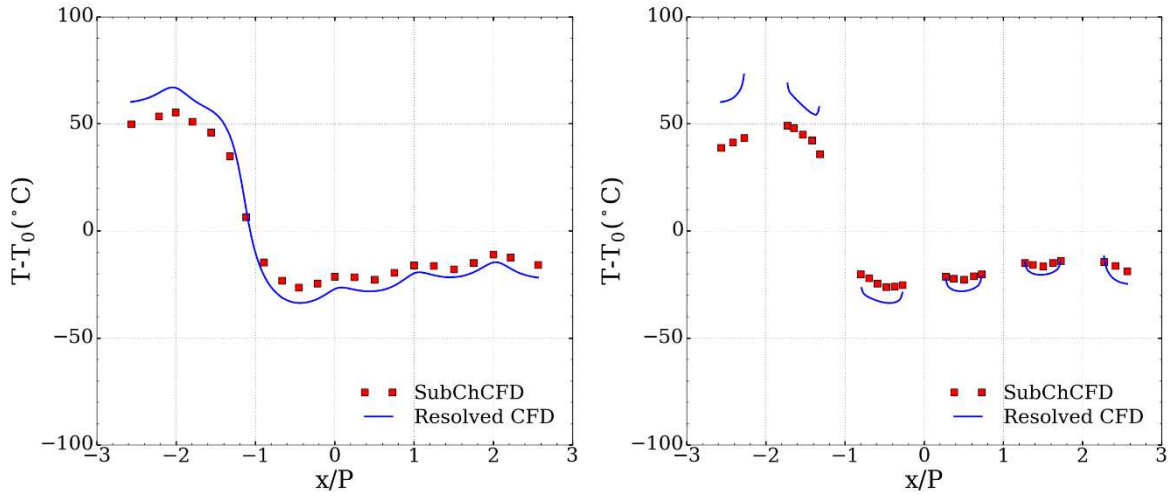

Fig. 14 Line plots of the velocity and temperature fields, (a) and (b) the normalised axial velocity over line 1 and line2, (c) and (d) the temperature over line 1 and line 2

3.2 Flow in a rod bundle with local blockage

The aforementioned test cases have demonstrated the feasibility of SubChCFD for calculations of fuel bundle flow and heat transfer. It is not only able to predict sub-channel-level behaviours but also to capture sub-scale physics within the sub-channels. Benefiting from the greatly reduced computing cost compared to resolved CFD, SubChCFD can be used for simulation of large-scale reactor components. In this section and the following one, we will further assess the performance of SubChCFD for full 3-D large-scale bundle flows.

The following case is used to test the capability of SubChCFD in tackling non-design operating circumstances. It is created by positioning a blockage in one of the sub-channels to obstruct the flow at a certain height in a 5×5 rod bundle. Geometrical details of the obstruction can be found in Figures 15 (a) and (b). During the operations in nuclear reactors, partial or complete blocking of single or multiple sub-channels of the reactor core is considered to be a credible scenario, for example, in PWR reactors due to LOCA-related rod swelling or ballooning (Creer et al., 1976). Due to the local blockage, the nearby coolant flow is significantly distorted, resulting in locally strengthened inter-channel mixing and lateral flow. The traditional sub-channel codes would find this very challenging due to the restrictions of the 1-D framework of formulation used. Some special treatment might be developed but it is impossible for such an approach to describe the 3-D flow phenomenon around the blockage and the large scale recirculation downstream in any detail. In contrast, SubChCFD is naturally suitable for this type of problem. Figure 15 (c) shows the extruded mesh of a cross-section passing through the blockage region,

which is generated based on the resolution of computing Mesh-2 described in Figure 3. The total amount of hexahedral cells for the entire 3-D SubChCFD model is about 0.645 million. This is much lower than that used in the CFD reference model which consists of as many as 21 million hexahedral mesh cells.

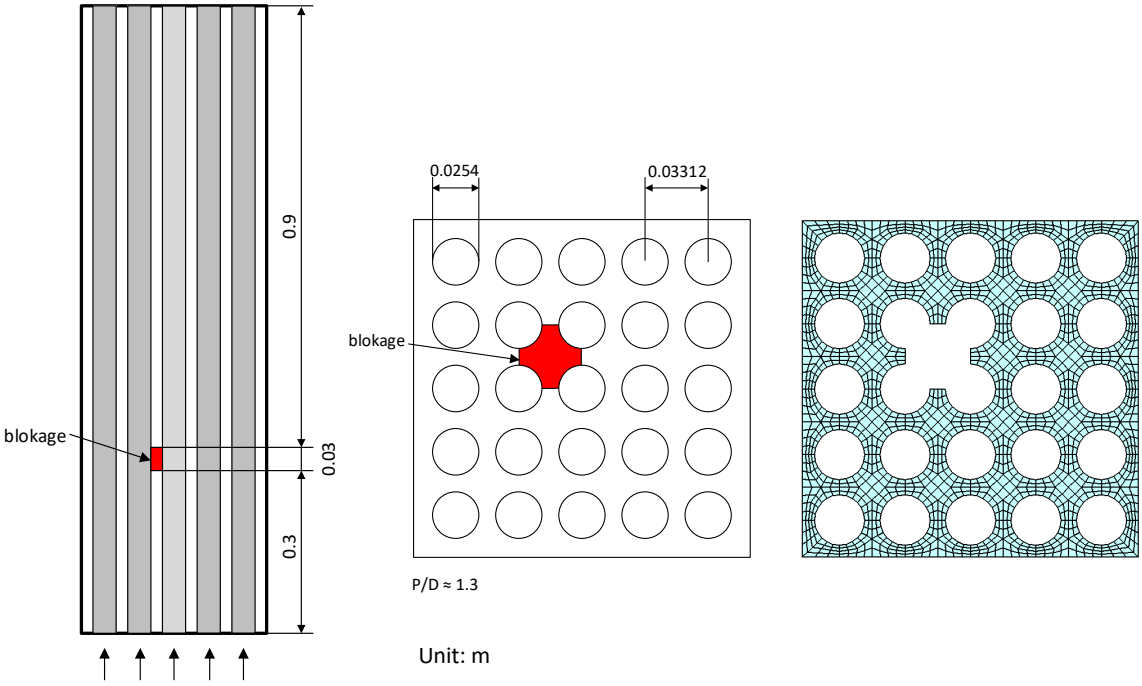

(a) (b) (c)

Fig. 15 Geometry and mesh of the 3-D rod bundle with local blockage, (a) and (b) the longitudinal and the cross-section view of the rod bundle (unit in m), (c) a cross-section of the computing mesh used in the SubChCFD model

Figure 16 shows comparisons between the simulation results produced using SubChCFD and the resolved CFD. The x-component of the cross-flow velocity is firstly plotted along a horizontal line (i.e. line-1 in Figure 16 a), which reflects the profile of the lateral flow distribution around the blockage area. It can be seen that SubChCFD produces very similar result to that of the resolved CFD. In this region, the Bernoulli's effect plays a leading role in shaping the local flow around the blockage, which can be just properly captured by SubChCFD. There are pressure losses due to re-circulation around the blockage, which are not currently modelled in SubChCFD. This lack does not affect the results significantly here, but the pressure losses could be accounted for in the model in the future. Figure 16 (c) shows the pressure distribution along line-2 shown in Figure 16 (a). As can be seen, the overall trend of the pressure variation is captured but some details, such as the appearance of the lower peak, cannot be reproduced with the SubChCFD simulations. Figure 16 (d) shows the axial pressure distribution along the centre line of sub-channel A (the sub-channel on the right-hand side close to the blockage, see sub-Figure 16 a). It is worth

noting that SubChCFD agrees very well with the resolved CFD in predicting the frictional loss of the non-blocked section and form loss of the blocked section, even though the local peak value is not accurately captured in comparison to the resolved simulation results. The sharp pressure dips are linked to the rapid local flow acceleration due to the reduced area. This is an inviscid effect and the pressure recovers and the velocity returns to its original value past the restricted flow area region, which explains why this effect is not captured by SubChCFD accurately, however, this sharp change, does not affect its overall performance.

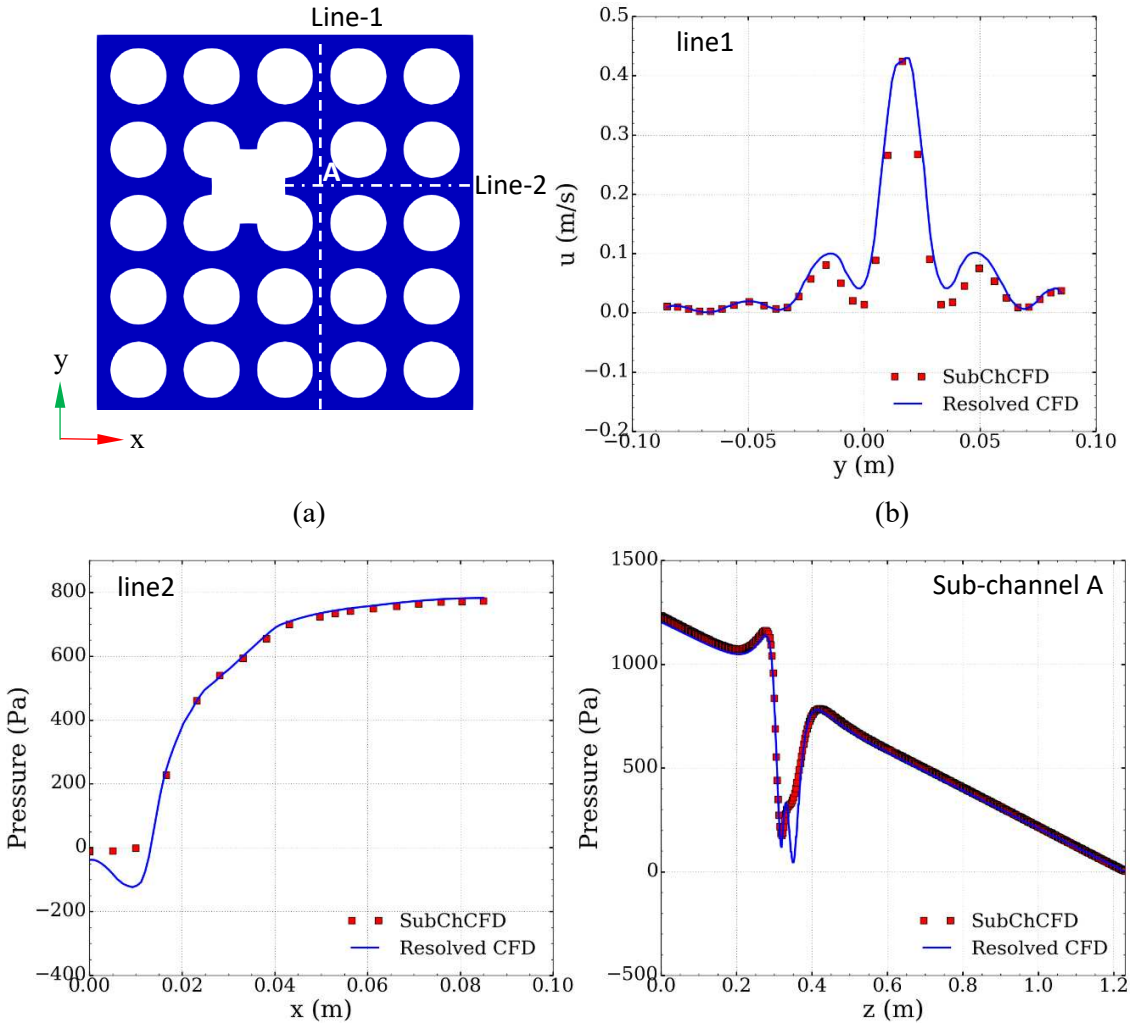

Fig. 16 Simulation results of the 3-D bundle with local blockage, (a) position of lines for plotting, (b) the x-direction velocity alone line-1, (c) the transverse pressure distribution alone line-2, (d) the axial pressure loss in sub-channel A

The computing cost was estimated in a similar way as that used in Section 3.1.2. However, simulations were not conducted in a serial manner due to the relatively large mesh size used in this case. Instead, they were run on a high performance computing (HPC) cluster. Considering the fact that the parallel speed-up of using Code_Saturne is in linear with the number of CPU processors, providing that each partition has no less than 10,000 to 20,000 cells (which is the case in the current investigation), the CPU time can be easily converted to an equivalent elapsed time of using only one processor. As such, the computing costs were estimated for both SubChCFD and resolved CFD, in which the former is about 190 times lower than the latter. It should be pointed out that the reduction in computing cost in such a full 3-D case is even lower than that of a 2-D case (see Section 3.1.2). This is mainly due to the use of a higher resolution mesh (Mesh-2 in Figure 3) for the SubChCFD simulation.

3.3 Flow in a two-parallel-assembly

The experimental test of flow in a two-14×14 parallel-assembly was carried out by Weiss and Markley (1971), aimed at investigating the flow redistribution between two open fuel assemblies resulting from a partial or full blockage at the entrance of one assembly. This case has also been studied numerically by S.J. Yoon et al. (2017) using their newly developed sub-channel code CUPID. This is a perfect case for direct comparisons between SubChCFD and the sub-channel codes used in large-scale component modelling.

The test section of the experimental rig consists of two 14×14 fuel assemblies interconnected through a water gap and enclosed in a rectangular housing (see Figure 17). Each of the assemblies is 0.1869 m in width and 0.1938 m in height, and the width of the water gap is 0.0155 m. The diameter of the rods is 0.0108 m and the pitch-to-diameter ratio is 1.28. The fuel assembly on the right-hand side is assumed to be partially blocked at the entrance, resulting in a reduced mass flux compared to the left assembly. In the numerical simulation, to reproduce the mass flow rates of 550 g/min and 1,110 g/min for the two bundles, inlet bulk velocities are set to 1.76 m/s and 3.52 m/s, respectively. For the water gap, the inlet velocity is assigned as 2.64 m/s.

Figure 18 shows the cross-section view of the computing mesh used for the parallel fuel assembly based on the resolution of Mesh-1 described in Figure 3. As can be seen from the zoomed-in inset, the distribution of the grid lines has been adjusted slightly in the edge sub-channels to improve the quality of the mesh elements close to the wall. Based on such resolution, a 3.3 million hexahedral cell mesh was generated for the entire 3-D model. A resolved CFD simulation for this case would need about 400 million cells, which is a large model even for current Tier-1/Tier-2 HPC research facilities. Instead of conducting a resolved CFD simulation, we evaluate the results of the SubChCFD by comparing them with those

obtained from the sub-channel code CUPID and the available experimental data. Figure 19 shows the axial velocity profiles at six different vertical elevations of the parallel assembly. They are plotted using mean values calculated through arithmetic averaging at three sampling locations in accordance to the experimental measuring points, located at the centre lines between row-2 and row-3, row-7 and row-8, and row-12 and row-13 of the fuel rods, respectively. For most of the levels (except level 2), the SubChCFD results agree somewhat better with the experimental data than those produced by CUPID. Moreover, as expected, SubChCFD provides more details of the flow profile than the traditional sub-channel code. For instance, the variation of the axial velocity occurring between the gap and the centre of the sub-channel are well captured. These variations appear to be smaller nearer the mixing interface as expected, where the strong cross flow and mixing smooth out the velocity gradients. Such phenomena cannot be predicted using a traditional sub-channel code.

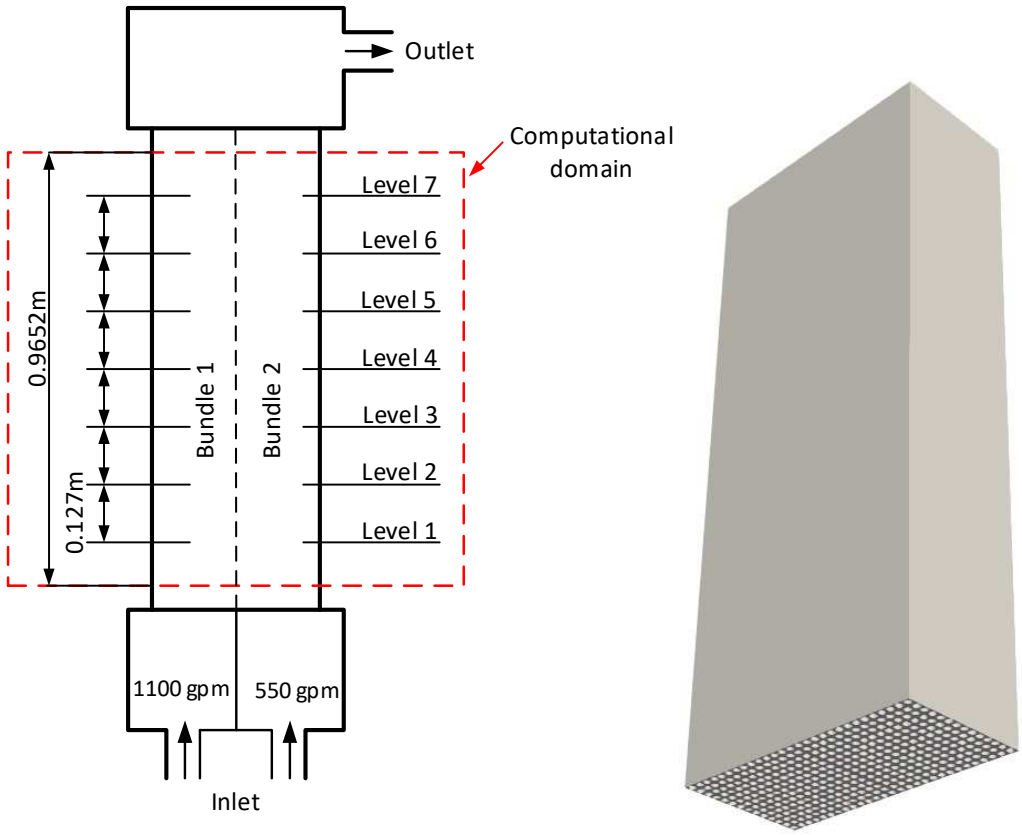

(a) (Yoon et al., 2017) (b)

Fig. 17 Modelling of the parallel fuel assembly, (a) schematic of the experimental facility, (b) numerical model of the test section

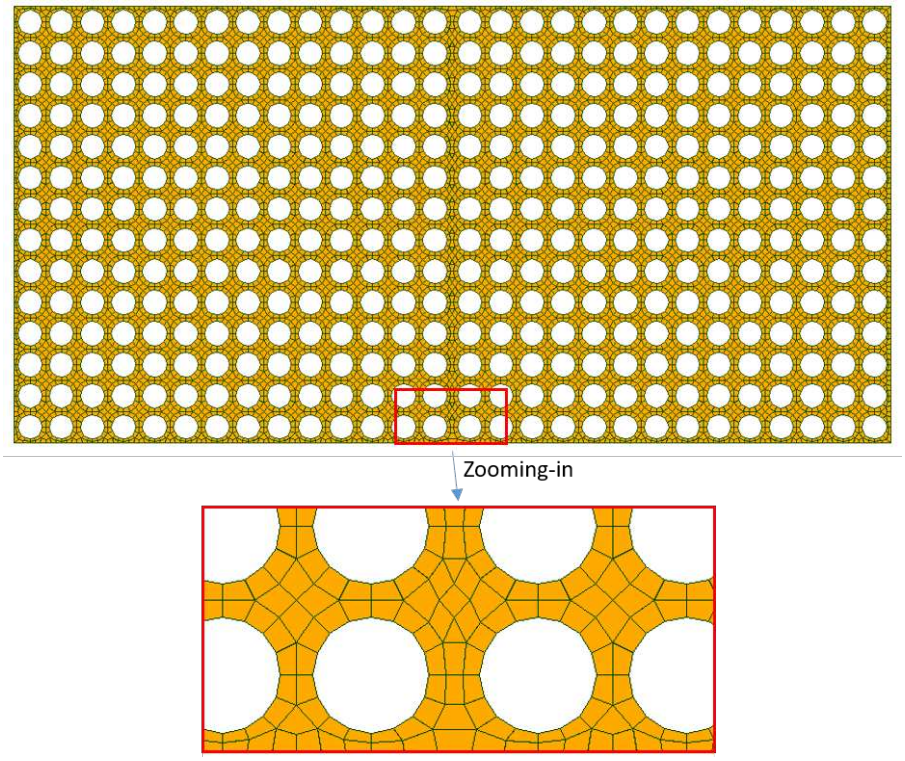

588

589 **Fig. 18 Cross section view of the computing mesh for the parallel assembly**

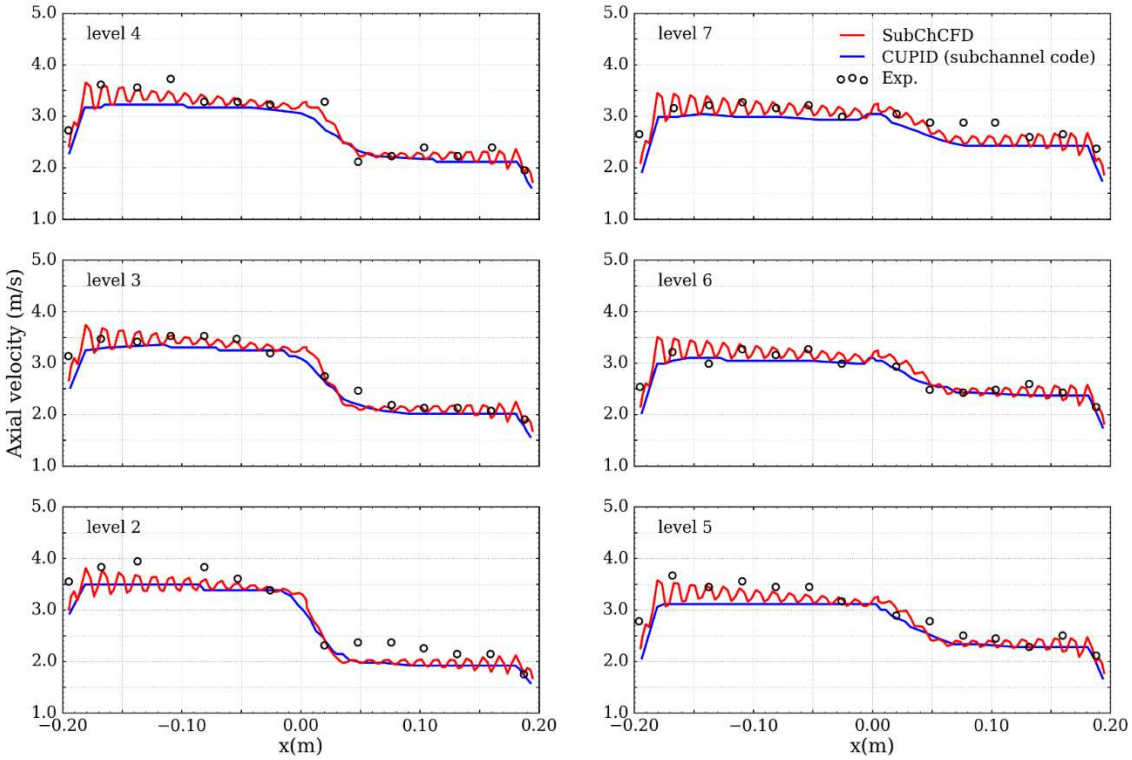

590

591 **Fig. 19 Axial mean velocity profiles of the parallel assembly**

4. Conclusions

A coarse-grid CFD-based, modern, sub-channel methodology (SubChCFD) has been developed to bridge the gap between the system/sub-channel codes and the conventional CFD. The convection term is directly discretised on the coarse mesh and the diffusion term is split into two parts, including the wall-boundary part and the interior part, respectively. The latter is then described using a simple turbulence model (a 0-equation mixing length turbulence model in this paper), whilst the former is tackled in a similar way as that is normally done in a sub-channel analysis code, using empirical correlations as closure laws. In doing so, on one hand, the computing cost is significantly reduced compared to conventional CFD methods due to the use of a coarse mesh, making it possible to simulate large reactor components or even the whole core. On the other hand, some advanced features of the conventional CFD are retained, including a full 3-D solution, high simulation robustness and application flexibility. SubChCFD can be readily coupled with resolved CFD or any other CFD-based methods (e.g. porous media approach), which is an important feature of this method. The former enables flexible local refinement in regions where the sub-grid flow phenomena are of interest. The latter can be used as a simple treatment of complex internal structures, such as spacer grids. Both will be explored as a follow-up of this work.

The methodology of SubChCFD has been implemented into the open-source CFD package Code_Saturne. A numerical test has then done for the 5×5 bare bundle of the OECD/NEA MATiS-H benchmarking experiment. It has been shown that SubChCFD has good numerical stability and robustness, and is able to capture the flow and heat transfer well in this axially dominant bundle flows, with a significant reduction in computing cost compared to conventional CFD.

Next, SubChCFD has been used to simulate two complex 3-D flow cases. The first case is a locally blocked rod bundle derived by placing an obstruction in one of the sub-channels. The cross-flow due to the blockage has been well captured and the predicted axial pressure loss due to friction and obstruction are in good agreement with those obtained from a resolved CFD simulation. The second case comprises two parallel fuel assemblies with different input mass flow rates. In this case, SubChCFD also produces excellent predictions, not only by successfully capturing the distribution of the axial velocity due to the inter-channel mixing but also by providing flow details within sub-channels which cannot be captured by the traditional sub-channel codes. In the future, SubChCFD will be further developed to broaden the scope of its application, including, for example, transverse-dominant flows, buoyancy-influenced mixed convection or natural circulation. Methods for coupling SubChCFD with resolved CFD and/or porous media method will also be explored.

Nomenclature

C_p	Specific heat, [J/(kg·℃)]
D	Rod diameter, [m]
D_h	Sub-channel hydraulic diameter, [m]
$\vec{e}_z$	Unit vector of the stream-wise direction
f	Skin frictional factor
$\overline{I}$	Unit tensor
l_m	The mixing length, [m]
$\vec{n}$	Outward normal vector of a cell surface
Nu	Sub-channel Nusselt number
$(\mathrm{Nu}_\infty)_{\mathrm{c.t.}}$	Nusselt number for a circular pipe at fully developed condition
p	Static pressure, [Pa]
P	Pitch of a rod array, [m]
Pr	Prandtl number
q	Heat flux of the rod surface, [W/m^2]
Re	Sub-channel Reynolds number
S_w	Cell surface that is adjacent to a wall boundary, [m^2]
S_f	Cell surface that is not adjacent to a wall boundary, [m^2]
S	Total cell surface, $S = S_w \bigcup S_f$, [m^2]
S_{ij}	Components of the strain rate tensor, [s^{-1}]
$\vec{S}_u$	Source term of the momentum equation, [N/m^3]
S_E	Source term of the energy equation, [W/m^3]
t	Time, [s]
T	Temperature, [℃]
T_0	Global bulk temperature, [℃]
T_b	Sub-channel bulk temperature, [℃]
T_w	Wall temperature, [℃]
$\vec{u}$	Velocity vector, [m/s]
u_0	Global bulk velocity, [m/s]
$\vec{u}_b$	Sub-channel bulk velocity vector, [m/s]
V_i	Volume of the i^{th} computing mesh cell, [m^3]
$V_{sub,j}$	Volume of the j^{th} filtering mesh cell, [m^3]

Greek symbols

Δ	Thickness of the boundary layer, [m]
δ	Kronecker notation
φ_i	CFD-level quantity of φ on the i^{th} computing mesh cell
$\varphi_{sub,j}$	Sub-channel-level quantity of φ on the j^{th} filtering mesh element
Φ_{net}	Net heat input to a flow domain, [J/s]
λ	Thermal conductivity, [W/(m·℃)]
λ_t	Turbulent thermal conductivity, [W/(m·℃)]
μ	Molecular viscosity, [Pa·s]
μ_t	Eddy viscosity, [Pa·s]
Ω	A cell of the computing mesh
Ω_d	The whole computational domain
Ω_{sub}	A cell of the filtering mesh

ρ	Fluid density, [kg/m^3]
$\overline{\sigma}$	Stress tensor, [Pa]
ψ	Correction factor of the Nusselt number for rod bundles

Acknowledgements

The present work was carried out as part of the R&D Program for Digital Reactor Design sponsored by the Department of Business, Energy and Industry Strategies (BEIS) of the UK (Grant reference number: TRN 1210/09/2016(3)). The authors would like to thank the STFC Hartree Centre for providing some of the compute time.

References

Agbodemegbe, V.Y., Cheng, X., Akaho, E.H.K., Allotey, F.K.A., 2016. An investigation of the effect of split-type mixing vane on extent of crossflow between subchannels through the fuel rod gaps. Ann. Nucl. Energy 88, 174–185. https://doi.org/10.1016/j.anucene.2015.10.036

Ala, A.A., Tan, S., Eltayeb, A., Zhengpeng, M., Xing, L., 2017. Simulation Study of Turbulent Flow Through 5x5 Rod Bundle, in: Proceedings of 17th International Topical Meeting on Nuclear Reactor Thermalhydraulics (NURETH-17). Xi'an.

Anderson, N., Hassan, Y., Schultz, R., 2008. Analysis of the hot gas flow in the outlet plenum of the very high temperature reactor using coupled RELAP5-3D system code and a CFD code. Nucl. Eng. Des. 238, 274–279. https://doi.org/10.1016/j.nucengdes.2007.06.008

Bavière, R., Tauveron, N., Perdu, F., Garré, E., Li, S., 2014. A first system/CFD coupled simulation of a complete nuclear reactor transient using CATHARE2 and TRIO-U. Preliminary validation on the Phénnix reactor natural circulation test. Nucl. Eng. Des. 277, 124–137. https://doi.org/10.1016/j.nucengdes.2014.05.031

Benhanmadouche, S., Moussou, P., Le Maitre, C., 2009. CFD estimation of the flow-induced vibrations of a fuel rod downstream a mixing grid, in: Proceedings of the ASME 2009 Pressure Vessels and Piping Division Conference. Prague, Czech Republic, pp. 1–9.

Bestion, D., 1990. The physical closure laws in the CATHARE code. Nucl. Eng. Des. 124, 229–245. https://doi.org/10.1016/0029-5493(90)90294-8

Bieder, U., 2017. Analysis of the IAEA-benchmark on flow mixing in a 4x4 rod bundle, in: Proceedings of 17th International Topical Meeting on Nuclear Reactor Thermalhydraulics (NURETH-17). Xi'an.

Bieder, U., Barthel, V., Ducros, F., Vandroux, S., 2010. CFD Calculations of Wire Wrapped Fuel Bundles: Modeling and Validation Strategies, in: CFD4NRS-3. Bethesda, USA, pp. 1–22.

Bieder, U., Falk, F., Fauchet, G., 2014. LES analysis of the flow in a simplified PWR assembly with

654 mixing grid. Prog. Nucl. Energy 75, 15–24. https://doi.org/10.1016/j.pnucene.2014.03.014
655 Brewster, R.A., Bissett, T.A., Xu, Y., 2017. Computational Fluid Dynamics Assessment of Baffle Plate
656 Leakage Flow Effects in a Downflow 4-Loop Reactor, in: Proceedings of 17th International Topical
657 Meeting on Nuclear Reactor Thermalhydraulics (NURETH-17). Xi'an.
658 Brockmeyer, L., Carasik, L.B., Merzari, E., Hassan, Y.A., 2016. CFD Investigation of Wire-Wrapped
659 Fuel Rod Bundle Inner Subchannel Behavior and Dependency on Bundle Size, in: Proceedings of
660 the 24th International Conference on Nuclear Engineering - ICONE 24. pp. 1–9.
661 https://doi.org/10.1007/978-3-319-58460-7_45
662 Bury, T., 2013. Coupling of CFD and lumped parameter codes for thermal-hydraulic simulations of
663 reactor containment. Comput. Assist. Methods Eng. Sci. 20, 195–206.
664 Chen, G., Zhang, Z., Tian, Z., Li, L., Dong, X., Ju, H., 2017. Design of a CFD scheme using multiple
665 RANS models for PWR. Ann. Nucl. Energy 102, 349–358.
666 https://doi.org/10.1016/j.anucene.2016.12.030
667 Chen, R., Tian, M., Chen, S., Tian, W., Su, G.H., Qiu, S., 2017. Three dimensional thermal hydraulic
668 characteristic analysis of reactor core based on porous media method. Ann. Nucl. Energy 104, 178–
669 190. https://doi.org/10.1016/j.anucene.2017.02.020
670 Chen, X., Du, S., Zhang, Y., Yu, H., Li, S., Peng, H., Wang, W., Zeng, W., 2017. Validation of CFD
671 analysis for rod bundle flow test with vaned spacer grids. Ann. Nucl. Energy 109, 370–379.
672 https://doi.org/10.1016/j.anucene.2017.05.055
673 Chen, Z., Chen, X.N., Rineiski, A., Zhao, P., Chen, H., 2015. Coupling a CFD code with neutron kinetics
674 and pin thermal models for nuclear reactor safety analyses. Ann. Nucl. Energy 83, 41–49.
675 https://doi.org/10.1016/j.anucene.2015.03.023
676 Class, A.G., Viellieber, M.O., Batta, A., Fax, T., 2011. Coarse-Grid-CFD for pressure loss evaluation in
677 rod bundles, in: Proceedings of ICAPP 2011. Nice, France, pp. 1773–1780.
678 Corzo, S., Ramajo, D., Nigro, N., 2015. 1/3D modeling of the core coolant circuit of a PHWR nuclear
679 power plant. Ann. Nucl. Energy 83, 386–397. https://doi.org/10.1016/j.anucene.2014.12.035
680 Creer, J.M., Rowe, D.S., Bates, J.M., Sutey, A.M., 1976. Effects of Sleeve Blockages on Axial Velocity
681 and Intensity of Turbulence in an Unheated 7 x 7 Rod Bundle. Battelle Pacific Northwest Labs.
682 Richland, Wash.(USA).
683 Cui, X.Z., Kim, K.Y., 2003. Three-dimensional analysis of turbulent heat transfer and flow through
684 mixing vane in a subchannel of nuclear reactor. J. Nucl. Sci. Technol. 40, 719–724.
685 https://doi.org/Doi 10.3327/Jnst.40.719
686 Denefle, R., Gauffre, M.C., Benhamadouche, S., 2017. CFD Study of Flow Redistributions in PWR Fuel
687 Assemblies, in: Proceedings of 17th International Topical Meeting on Nuclear Reactor

688 Thermalhydraulics (NURETH-17). Xi'an.
689 Dittus, W., Boelter, L.M.K., 1985. Heat Transfer in Automobile Radiators of the Tubular Type. Int.
690 Commun. Heat Mass Transf. 12, 3–22. https://doi.org/10.1021/acs.jproteome.6b00648
691 Fiorina, C., Clifford, I., Aufiero, M., Mikityuk, K., 2015. GeN-Foam: A novel OpenFOAM® based multi-
692 physics solver for 2D/3D transient analysis of nuclear reactors. Nucl. Eng. Des. 294, 24–37.
693 https://doi.org/10.1016/j.nucengdes.2015.05.035
694 Fischer, P., Lottes, J., Siegel, A., Palmiotti, G., 2007. Large eddy simulation of wire-wrapped fuel pins I:
695 Hydrodynamics in a Periodic Array, in: Joint International TopicalMeeting onMathematics &
696 Computation and Supercomputing in Nuclear Applications (M&C + SNA 2007). Monterey,
697 California.
698 Fournier, Y., Bonelle, J., Moulinec, C., Shang, Z., Sunderland, A.G., Uribe, J.C., 2011. Optimizing
699 Code_Saturne computations on Petascale systems. Comput. Fluids 45, 103–108.
700 https://doi.org/10.1016/j.compfluid.2011.01.028
701 Grunloh, T.P., Manera, A., 2016. A novel domain overlapping strategy for the multiscale coupling of
702 CFD with 1D system codes with applications to transient flows. Ann. Nucl. Energy 90, 422–432.
703 https://doi.org/10.1016/j.anucene.2015.12.027
704 Han, B., Wang, B., Zhou, Z., Zha, Y., 2017. Numerical study on the effect of grid mixing span in 2×1
705 spacer grid, in: Proceedings of 17th International Topical Meeting on Nuclear Reactor
706 Thermalhydraulics (NURETH-17). Xi'an.
707 Hanna, B.N., Dinh, N.T., Youngblood, R.W., Bolotnov, I.A., 2017. Coarse-Grid Computational Fluid
708 Dynamic (CG-CFD) Error Prediction using Machine Learning. arXiv Prepr. arXiv1710.09105.
709 Házi, G., 2005. On turbulence models for rod bundle flow computations. Ann. Nucl. Energy 32, 755–761.
710 https://doi.org/10.1016/j.anucene.2004.12.012
711 Hu, R., Fanning, T.H., 2013. A momentum source model for wire-wrapped rod bundles - Concept,
712 validation, and application. Nucl. Eng. Des. 262, 371–389.
713 https://doi.org/10.1016/j.nucengdes.2013.04.026
714 Hwang, D.H., Seo, K.W., Kwon, H., 2008. Validation of a Subchannel Analysis Code MATRA Version
715 1.0. Korea Atomic Energy Research Institute.
716 Ikeda, K., 2014. CFD application to advanced design for high efficiency spacer grid. Nucl. Eng. Des. 279,
717 73–82. https://doi.org/10.1016/j.nucengdes.2014.02.013
718 Imaizumi, M., Ichioka, T., Hoshi, M., Teshima, H., Kobayashi, H., Yokoyama, T., 1995. Development of
719 CFD method to evaluate 3-D flow characteristics for PWR fuel assembly, in: Transactions of the
720 13th International Conference on Structural Mechanics in Reactor Technology. Porto Alegre, pp. 1–
721 12.

722 Jeong, H.-Y., Ha, K.-S., Chang, W.-P., Kwon, Y.-M., Lee, Y.-B., 2005. Modeling of Flow Blockage in a
723 Liquid Metal-Cooled Reactor Subassembly with a Subchannel Analysis Code. Nucl. Technol. 149,
724 71–87. https://doi.org/10.13182/NT05-A3580
725 Kang, S.K., Hassan, Y.A., 2016. Computational fluid dynamics (CFD) round robin benchmark for a
726 pressurized water reactor (PWR) rod bundle. Nucl. Eng. Des. 301, 204–231.
727 https://doi.org/10.1016/j.nucengdes.2016.03.007
728 Kao, M.-T., Lee, M., Ferng, Y.-M., Chieng, C.-C., 2010. Heat transfer deterioration in a supercritical
729 water channel. Nucl. Eng. Des. 240, 3321–3328. https://doi.org/10.1016/j.nucengdes.2010.06.028
730 Kao, M., Wu, C., Chieng, C., Xu, Y., Yuan, K., Dzodzo, M.B., Conner, M.E., Beltz, S., Ray, S., Bissett,
731 T., 2010. CFD Analysis of PWR Reactor Vessel Upper Plenum Sections- Flow Simulation in
732 Control Rods Guide Tubes, in: Proceedings of the 18th International Conference on Nuclear
733 Engineering (ICONE18). Xi'an, pp. 1–8. https://doi.org/10.1115/ICONE18-29466
734 Kao, M.T., Wu, C.Y., Chieng, C.C., Xu, Y., Yuan, K., Dzodzo, M., Conner, M., Beltz, S., Ray, S., Bissett,
735 T., 2011. CFD analysis of PWR core top and reactor vessel upper plenum internal subdomain models.
736 Nucl. Eng. Des. 241, 4181–4193. https://doi.org/10.1016/j.nucengdes.2011.08.007
737 Karouta, Z., GU, C.-Y., Schoelin, B., 1995. 3-D flow analyses for design of nuclear fuel spacer, in:
738 Proceedings of 7th International Meeting on Nuclear Reactor Thermal-Hydraulics. New York.
739 Lerchl, G., Austregesilo, H., Glaeser, H., Hrubisko, M., Luther, W., 2012. ATHLET MOD3.0 Cycle A.
740 https://www.grs.de/sites/default/files/fue/ATHLET-Overview.pdf.
741 Liles, D.R., Mahaffy, J.H., 1986. TRAC-PF1/MOD1: An Advanced Best-estimate Computer Program for
742 Pressurized Water Reactor Thermal-hydraulic Analysis, NUREG/CR-3858. Los Alamos National
743 Lab, NM (USA), Safety Code Development Group.
744 Liu, C.C., Ferng, Y.M., 2010. Numerically simulating the thermal-hydraulic characteristics within the
745 fuel rod bundle using CFD methodology. Nucl. Eng. Des. 240, 3078–3086.
746 https://doi.org/10.1016/j.nucengdes.2010.05.021
747 Liu, C.C., Ferng, Y.M., Shih, C.K., 2012. CFD evaluation of turbulence models for flow simulation of
748 the fuel rod bundle with a spacer assembly. Appl. Therm. Eng. 40, 389–396.
749 https://doi.org/10.1016/j.applthermaleng.2012.02.027
750 Moorthi, A., Kumar Sharma, A., Velusamy, K., 2018. A review of sub-channel thermal hydraulic codes
751 for nuclear reactor core and future directions. Nucl. Eng. Des. 332, 329–344.
752 https://doi.org/10.1016/j.nucengdes.2018.03.012
753 Papukchiev, A., Lerchl, G., Weis, J., Scheuerer, M., Austregesilo, H., 2011. Development of a coupled
754 1D-3D Thermal-Hydraulic Code for Nuclear Power Plant Simulation and its Application to a
755 Pressurized Thermal Shock Scenario in PWR, in: Proceedings of 14th International Topical Meeting

on Nuclear Reactor Thermalhydraulics Conference (NURETH-14). Toronto.

Podila, K., Bailey, J., Rao, Y.F., Krause, M., 2013. A CFD simulation of 5X5 rod bundles with split-type spacers, in: 2013 21st International Conference on Nuclear Engineering (ICONE21). American Society of Mechanical Engineers, p. V004T09A027-V004T09A027.

RELAP5 Development Team, 1995. RELAP5/MOD3 Code Manual Code Structure, System Models, and Solution Methods. Idaho National Engineering Laboratory, Lockheed Idaho Technologies Company, Idaho Falls, Idaho.

Roelofs, F., Gopala, V.R., Chandra, L., Viellieber, M., Class, A., 2012. Simulating fuel assemblies with low resolution CFD approaches. Nucl. Eng. Des. 250, 548–559. https://doi.org/10.1016/j.nucengdes.2012.05.029

Rowe, D.S., 1967. Cross-flow mixing between parallel flow channels during boiling part I COBRA - computer program for coolant boling in rod arrays. Battelle-Northwest, Richland, Wash. Pacific Northwest Lab.

Sha, W.T., 1980. An overview on rod-bundle thermal-hydraulic analysis. Nucl. Eng. Des. 62, 1–24. https://doi.org/10.1016/0029-5493(80)90018-7

Shams, A., Roelofs, F., Komen, E.M.J., Baglietto, E., 2013. Quasi-direct numerical simulation of a pebble bed configuration. Part I: Flow (velocity) field analysis. Nucl. Eng. Des. 263, 473–489. https://doi.org/10.1016/j.nucengdes.2012.06.016

Simoneau, J.P., Champigny, J., Mays, B., Lommers, L., 2007. Three-dimensional simulation of the coupled convective, conductive, and radiative heat transfer during decay heat removal in an HTR. Nucl. Eng. Des. 237, 1923–1937. https://doi.org/10.1016/j.nucengdes.2007.03.010

Skibin, A.P., Volkov, V.Y., Golibrodo, L.A., Krutikov, A.A., Kudryavtsev, O. V, Nadinskiy, Y.N., Gidropress, O.K.B., 2017. Development of CFD-Model of AES-2006 Reactor, in: Proceedings of 17th International Topical Meeting on Nuclear Reactor Thermalhydraulics (NURETH-17). Xi'an.

Smith, B.L., Song, C.-H., Chang, S.-K., Lee, R.J., Kim, J.W., 2013. Report of the OECD/NEA KAERI Rod Bundle CFD Benchmark Exercise. Rep. NEA/CSNI/R.

Stewart, C.W., Cuta, J.M., Koontz, A.S., Kelly, J.M., Basehore, K.L., George, T.L., Rowe, D.S., 1983. VIPRE-01: A Thermal-Hydraulic Analysis Code for Reactor Cores Volume 1. Mathmatical Modeling. [PWR; BWR] No. EPRI-NP-2511-CCM-Vol. 1. Battelle Pacific Nort.

Takamatsu, K., 2017. Thermal-hydraulic analyses of the High-Temperature engineering Test Reactor for loss of forced cooling at 30% reactor power. Ann. Nucl. Energy 106, 71–83. https://doi.org/10.1016/j.anucene.2017.03.032

Todreas, N.E., Kazimi, M.S., 1990. Nuclear Systems I: Thermal Hydraulic Fundamentals. Taylor & Francis.

Toti, A., Vierendeels, J., Belloni, F., 2017. Improved numerical algorithm and experimental validation of a system thermal-hydraulic/CFD coupling method for multi-scale transient simulations of pool-type reactors. Ann. Nucl. Energy 103, 36–48. https://doi.org/10.1016/j.anucene.2017.01.002

Tseng, Y.S., Ferng, Y.M., Lin, C.H., 2014. Investigating flow and heat transfer characteristics in a fuel bundle with split-vane pair grids by CFD methodology. Ann. Nucl. Energy 64, 93–99. https://doi.org/10.1016/j.anucene.2013.09.037

Tsuji, N., Nakano, M., Takada, E., Tokuhara, K., Ohashi, K., Okamoto, F., Tazawa, Y., Inaba, Y., Tachibana, Y., 2014. Study of the applicability of CFD calculation for HTTR reactor. Nucl. Eng. Des. 271, 564–568. https://doi.org/10.1016/j.nucengdes.2013.12.033

Viellieber, M., Class, A.G., 2012. Anisotropic porosity formulation of the coarse-grid-CFD (CGCFD), in: Proceedings of the 2012 20th International Conference on Nuclear Engineering Collocated with the ASME 2012 Power Conference ICONE20-POWER2012. California, pp. 1–11.

Weiss, E., Markley, R.A., 1971. Open duct cooling-concept for the radial blanket region of a fast breeder reactor. Nucl. Eng. Des. 16, 375–386.

Yadigaroglu, G., Andreani, M., Dreier, J., Coddington, P., 2003. Trends and needs in experimentation and numerical simulation for LWR safety. Nucl. Eng. Des. 221, 205–223. https://doi.org/10.1016/S0029-5493(02)00339-4

Yoon, S.J., Kim, S.B., Park, G.C., Yoon, H.Y., Cho, H.K., 2017. Application of Cupid for Subchannel-Scale Thermal-Hydraulic Analysis of Pressurized Water Reactor Core Under Single-Phase Conditions. Nucl. Eng. Technol. 50, 54–67. https://doi.org/10.1016/j.net.2017.09.008

Yu, F., Class, A., Xiao, J., Jordan, T., 2017. Coarse grid CFD methodology: flux corrections for individual mesh cells and application to rod bundles, in: Proceedings of 17th International Topical Meeting on Nuclear Reactor Thermalhydraulics (NURETH-17). Xi'an.

Yu, Y., Merzari, E., Obabko, A., Thomas, J., 2015. A porous medium model for predicting the duct wall temperature of sodium fast reactor fuel assembly. Nucl. Eng. Des. 295, 48–58. https://doi.org/10.1016/j.nucengdes.2015.09.020

Zhang, G., Yang, Y.H., Gu, H.Y., Yu, Y.Q., 2013. Coolant distribution and mixing at the core inlet of PWR in a real geometry. Ann. Nucl. Energy 60, 187–194. https://doi.org/10.1016/j.anucene.2013.05.008

Zhao, H., Yang, B., Zha, Y., 2017. Analysis of the Three Dimension Flow Field of Single and Multi-Span Fuel Assemblies, in: Proceedings of 17th International Topical Meeting on Nuclear Reactor Thermalhydraulics (NURETH-17). Xi'an.